A RIGOROUS COMPRESSIBLE STREAMLINE FORMULATION FOR BLACK OIL AND COMPOSITIONAL SIMULATION

A Dissertation

by

ICHIRO OSAKO

Submitted to the Office of Graduate Studies of
Texas A&M University
in partial fulfillment of the requirements for the degree of

DOCTOR OF PHILOSOPHY

December 2006

Major Subject: Petroleum Engineering

A RIGOROUS COMPRESSIBLE STREAMLINE FORMULATION FOR BLACK OIL AND COMPOSITIONAL SIMULATION

A Dissertation

by

ICHIRO OSAKO

Submitted to the Office of Graduate Studies of
Texas A&M University
in partial fulfillment of the requirements for the degree of

DOCTOR OF PHILOSOPHY

Approved by:

Chair of Committee,	Akhil Datta-Gupta
Committee Members,	Daulat D. Mamora
	Ding Zhu
	Yalchin Efendiev
Head of Department,	Steve A. Holditch

December 2006

Major Subject: Petroleum Engineering

ABSTRACT

A Rigorous Compressible Streamline Formulation for Black Oil and Compositional Simulation.

(December 2006)

Ichiro Osako, B.E., Waseda University;

M.S., Texas A&M University

Chair of Advisory Committee: Dr. Akhil Datta-Gupta

In this study for the first time we generalize streamline models to compressible flow using a rigorous formulation while retaining most of its computational advantages. Our new formulation is based on three major elements and requires only minor modifications to existing streamline models. First, we introduce a relative density for the total fluids along the streamlines. This density captures the changes in the fluid volume with pressure and can be conveniently and efficiently traced along streamlines. Thus, we simultaneously compute time of flight and volume changes along streamlines. Second, we incorporate a density-dependent source term in the streamline saturation/composition conservation equation to account for compressibility effects. Third, the relative density, fluid volumes and the time-of-flight information are used to incorporate cross-streamline effects via pressure updates and remapping of saturations. Our proposed approach preserves the 1-D nature of the conservation calculations and all the associated advantages of the streamline approach. The conservation calculations are fully decoupled from the underlying grid and can be carried out using large time steps without grid-based stability limits.

We also extend the streamline simulation to compositional modeling including compressibility effects. Given the favorable computational scaling properties of streamline models, the potential advantage for compositional simulation can be even more compelling. Although several papers have discussed compositional simulation formulation, they all suffer from a major limitation, particularly for compressible flow. All of the previous works assume, either explicitly or implicitly, that the divergence of total flux along streamlines is negligible. This is not only incorrect for compressible flow but also introduces inconsistency between the pressure and conservation equations. We examine the implications of these assumptions on the accuracy of compositional streamline simulation using a novel and rigorous treatment of compressibility.

We demonstrated the validity and practical utility of our approach using synthetic and field examples and comparison with a finite difference simulator. Throughout the validation for compositional model, we found out the importance of finer segments discretizations along streamlines. We introduce optimal coarsening of segments to minimize flash calculations on each segment while keeping the accuracy of finer segments.

DEDICATION

This dissertation is dedicated to my lovely wife, Satoko, and my family in Japan, especially to my parents, Hitoshi and Yoko, and my brother, Takuro, and grandmother, Chiyoko for their love, care and encouragement.

ACKNOWLEDGMENTS

I would like to take this opportunity to express my deepest gratitude and appreciation to my advisor and committee chair, Dr. Akhil Datta-Gupta, for his continuous encouragement and especially for his academic guidance. Also, I would like to extend my sincere thanks to Dr. Daulat Mamora, Dr. Ding Zhu, and Dr. Yalchin Efendiev for serving as committee members.

I would like to acknowledge Dr. Michael J. King in BP America, Inc for his academic guidance and the helpful discussion.

I would like to acknowledge Chevron Energy Technology Company for providing me a lot of experiences and the opportunity to apply my technical knowledge during my summer internship. I would like to thank my mentors: Muu Hoang, Alex Castellini, Cengiz Satik, and Mridul Kumar.

I would like to thank all members of Dr. Arihara's research group in Waseda University [Especially for Dr. Norio Arihara and Sutopo-hakase (now with Institut Teknologi Bandung)] for their continuous encouragement from Japan.

Finally, I want to thank my friends in the 'Model Calibration and Efficient Reservoir Imaging (MCERI)' group, Dr. Arun Kharghoria, Dr. Sangheon Lee, Dr. Dr. Zhong He, Harshal Parikh, Hector Perez, Dr. Ahmed Daoud, Dr. Hao Cheng, Il Nam, Dr. Leonardo Vega, Dr. Mishal Al-Harbi, Chengwu Yuan, Elkin Arroyo, Fady Chaban, Ahmed Al-Hutheli, Eduardo Jimenez, Deepak Devegowda, Jong Uk Kim, Ajitabh Kumar, Xianlin Ma, Dayo Oyerinde, Rahul Mukerjee, and Eileen Paclibon, for many great memory during my graduate studies in Texas A&M University.

I would like to acknowledge financial support from the Joint Industry Project members and also from the U.S. Department of Energy. The facilities and resources provided by the Harold Vance Department of Petroleum Engineering of Texas A&M University are gratefully acknowledged.

TABLE OF CONTENTS

CHAPTER Page

LIST OF TABLES

LIST OF FIGURES

FIGURE Page

FIGURE Page

CHAPTER I

INTRODUCTION

1.1 Statement of the Problem

Streamline simulators have received increased attention in the petroleum industry because of their ability to effectively handle multimillion cell detailed geologic models and large simulation models. The efficiency of streamline simulation has relied primarily on the decoupling of the 3-D conservation equation into 1-D equations along streamlines using the streamline time of flight as the spatial coordinate.[1] Until now, this decoupling has been strictly valid for incompressible flow. Applications to compressible flow have generally lacked strong theoretical foundations and for the most part yielded mixed or unsatisfactory results.

In this study for the first time we generalize streamline models to compressible flow using a rigorous streamline formulation while retaining much of its favorable characteristics.[2] Our new formulation is based on three major elements and requires only minor modifications to existing streamline models. First, we introduce an 'effective density' for the total fluids along the streamlines. This density captures the changes in the fluid volume with pressure and can be conveniently and efficiently traced along streamlines. Thus, we simultaneously compute time of flight and volume changes along streamlines. Second, we incorporate a density-dependent source term in the streamline conservation equation to account for compressibility effects. Third, the effective density, fluid volumes and the time-of-flight information are used to incorporate cross-streamline effects via pressure updates and remapping of saturations/compositions evolved using the conservation equation. Our proposed approach preserves the 1-D nature of the saturation/composition update calculations and all the associated advantages of the streamline approach. The conservation calculations are fully decoupled from the underlying grid and can be carried out using large time steps without grid-based stability limits.

We demonstrated the validity and practical utility of our approach using synthetic and field examples and comparison with both commercial finite difference and streamline simulators for

---

This dissertation follows the style and format of the *SPE Journal*.

black oil model. The synthetic examples involve waterflooding in a ¼-five spot pattern under undersaturated conditions and also three phase flow with both free and solution gas. Our results show close agreement with the finite difference simulator in terms of water-oil and gas-oil ratio histories for an extended period of time. The field example is from a highly heterogeneous carbonate reservoir in West Texas and includes multiple patterns consisting of 11 injectors, 31 producers and over 30 years of production history. Our proposed formulation results in significant improvement in performance prediction over current commercial streamline simulators.

In many applications, a black oil representation of the reservoir fluids is inadequate. These include depletion of gas condensate and volatile oil reservoirs and also enhanced oil recovery processes such as enriched miscible gas injection, carbon dioxide flooding and chemical flooding. Specifically, when the fluid properties are dependent on both phase composition and pressure, we have to resort to compositional simulation. Such simulations involve the solution of the mass conservation equation in conjunction with phase equilibrium calculations to determine phase compositions, phase pressures and saturations.[3-5] The additional capabilities of compositional simulation also make it more expensive in terms of computation time and memory. This makes the potential benefit of streamline based compositional simulation even more compelling than for black oil or for two phase waterflood. In this study, we derive 1-D conservation equation for compositional model and apply the equation into academic finite difference compositional simulator (UTCOMP).[6] Thus, pressure and phase equilibrium calculations are obtained from the simulator and our new approach is used in conservation equation part evolving compositions. We will validate and utilize our new approach using synthetic 2-D homogeneous and 3-D heterogeneous examples by comparing our compositional streamline simulator with the finite difference simulator.

Through the application of compositional streamline simulation, we found out the necessity of finer discretization of segments along streamline. Maintaining the finer discretization is very expensive in terms of computational cost because flash calculations are conducted on each discretized segments along streamline. As we increase the number of segments to keep finer discretization, the computational time will also increase significantly. To overcome the problem we introduce optimal coarsening of streamline segments based on optimal upgridding technique widely applied in geological parameters.[7] The simple statistical criteria accounting for trade off between bias and variance can coarsen some segments while keeping finer discretizations in

necessary segments such as near injection/production wells and saturation fronts. We will illustrate our new approach using a synthetic 1D example and also utilize it using same synthetic 2-D homogeneous and 3-D heterogeneous examples for the validation of compositional model. Our approach will enable us to reduce computational time significantly and we will examine CPU time comparison with finite difference simulator to see scaling effect of our streamline simulation.

1.2 Background and Literature Review

Streamline simulators have become increasingly popular for high resolution reservoir simulation using multimillion cell geologic models. For incompressible or slightly compressible flow and under convection dominated conditions, streamline models are well-known to outperform conventional finite-difference simulation in terms of computational speed.[1,8-10] Streamline models can also result in improved accuracy because of subgrid resolution and reduced numerical dispersion and grid orientation effects.[8] To a large extent, the efficiency of the current streamline formulation is the consequence of the incompressibility assumption that allows us to easily and effectively decouple the pressure and conservation equations during flow simulation. This decoupling has been greatly facilitated by the introduction of the streamline time of flight coordinate.[1] Specifically, utilizing the time of flight as the spatial coordinate, the multidimensional conservation equations are reduced to a series of 1-D solutions along streamlines. These 1-D solutions can be carried out independently and using relatively large time-steps as they are not impacted by the underlying geologic grid-based stability limitations. This is the primary advantage of the streamline simulation. In addition, for heterogeneity dominated flow and adverse mobility ratio conditions, the streamlines need to be updated infrequently, leading to further savings in computation time.[9]

However, much of the elegance and simplicity of the current streamline formulation is lost when we consider compressible flow. This is because the pressure and conservation equations are now strongly coupled. Also, compressibility effects will require more frequent pressure recalculations to account for unsteady state effects and also to adequately update pressure dependent reservoir properties. Several authors have attempted to incorporate compressibility effects during streamline simulation.[11-15] Most of these previous works have rigorously accounted for compressibility effects during the pressure and velocity calculations using

standard finite-difference formulation.[12-15] However, while deriving the conservation equations along streamlines, all of these formulations fail to adequately account for compressibility effects. This is because of the inherent assumptions behind the current streamline time of flight formulation. All of the previous works on compressible streamline simulation assume, either explicitly or implicitly, that the divergence of total flux along streamlines is negligible. This is not only incorrect for compressible flow but also introduces inconsistency between the pressure and conservation equations. All these lead to increased material balance error and very often inaccurate performance predictions. Our experience with compressible flow in the current commercial streamline simulators has been mixed; problems with the formulation are probably quite widespread.

1.3 Objectives of Research

The primary objective of this research is to overcome problems obtained by conventional streamline simulations by presenting a rigorous streamline formulation for compressible black oil and compositional flow. Followings are the basic objectives:

- Introduce the compressible streamline formulation and highlight the main differences with the existing incompressible formulation.

- Present several examples to outline the major steps and illustrate the underlying concepts in compressible streamline simulation.

- Derive the 1-D saturation equations along streamlines for compressible black oil model.

- Examine the stability and time step selection for pressure updates during compressible black oil model.

- Derive the 1-D conservation equations along streamlines for compositional model.

- Introduce optimal coarsening of segments along streamlines to reduce computational time while retaining the accuracy of finer discretization segments results.

- Validate and demonstrate the practical use of our approaches

1.4 Dissertation Outline

Chapter II discusses the general background of streamline simulation and extension to compressible flow. Streamline simulation starts from the pressure equation. We calculate velocity field from the pressure, then we can trace the streamline. The essence of streamline simulation is to decouple the conservation equation from 3-D space into 1-D "time of flight" as the spatial coordinate. However, the decoupling of the conservation equation arises from the inherent assumption of incompressibility which provides a lot of advantages in conventional streamline simulation. We will discuss how we overcome the inherent assumption with the new approach.

In Chapter III, we will extend our approach to the application of two- and three- phase black oil model. The conventional streamline simulation has mainly involved applications to incompressible or slightly compressible flow. We demonstrate how our approach works when we apply it to more compressible oil and gas phases. In the presence of gas, gravity segregation is one of the major mechanisms in the reservoir. We demonstrate how we can handle the gravity segregation in streamline simulation using operator splitting technique.

In Chapter IV, we will extend our approach to compositional model. In some practical applications such as depletion of gas condensate and volatile oil reservoirs and also enhanced oil recovery processes, a black oil model is not enough to represent the actual reservoir fluid components. However, compositional simulation requires more computational time. As the computation time increases, the streamline approach can be more advantageous. We apply our approach to compositional simulation and demonstrate its advantages using synthetic examples.

In Chapter V, we introduce a method to optimize coarsening of the number of segments along streamlines for 1-D transport calculations. If we refine the number of discretization segments to evolve compositions along streamlines, it results in better accuracy, however, it will also increase the computational time because increased the number of flash calculations along streamlines. The optimal coarsening method enables us to coarsen segments in regions that do not require finer resolution such as far from wells and saturations fronts while retaining the accuracy of the finer resolution else where. We will illustrate the method with simple 1-D gas injection problem and validate it for 2-D homogeneous and 3-D heterogeneous cases.

In Chapter VI, the new developments from this work and their practical applicability are summarized. Potential future research works are also suggested.

CHAPTER II

A RIGOROUS COMPRESSIBLE FORMULATION*

Much of the elegance of the current streamline (or streamtube) formulation arises from the restriction to incompressible flow. In short, if a specific volumetric flux is allocated to a line or a tube at an injector, then that same flux will be transported to a producer. However, most real systems have some degree of compressibility. The compressibility effects become particularly important for three-phase flow including gas. Thus, the formulation needs to be generalized to account for changes in fluid volumes because of pressure variations along the streamwise directions. Fortunately, a small modification to the equations presented so far can be used to determine the volumetric flux as a function of distance along a streamline. A similar approach could be applied to streamtube calculations, although historically this has not been implemented. This chapter explains from the background of streamline including inherent incompressible assumptions to the extension to compressible fluid flow.

2.1 Streamline Simulation Background

We will first start with a brief review of the current streamline formulation before discussing its extensions to compressible flow. At a fundamental level, all streamline techniques are based upon a coordinate transformation from physical space to a coordinate system following the flow directions. This transformation is based upon the bi-streamfunctions and an additional time of flight coordinate. Following Bear [16] we introduce the bi-streamfunctions, ψ, and χ to construct a velocity field, $\vec{u}$,

$$\vec{u} = \nabla\psi \times \nabla\chi \quad \text{.....} \quad (2.1)$$

---

* Part of this chapter is reprinted with permission from "A Rigorous Compressible Streamline Formulation for Two and Three-Phase Black Oil Simulation," by Hao Cheng, Ichiro Osako, Akhil Datta-Gupta, and Michael J. King, paper SPE 96866 presented at the 2005 SPE Annual Technical Conference and Exhibition, Dallas, TX, October 9-12, Copyright 2005 by the Society of Petroleum Engineers.

Note that the incompressibility assumption is implicit in the definition of the bi-streamfunctions because of the vector identity,

$$\nabla \bullet (\nabla \psi \times \nabla \chi) = 0 \quad \text{.....} \tag{2.2}$$

A streamline is defined by the intersection of a constant value for ψ with a constant value for χ. In two dimensional applications, we use the simplified functional forms, $\psi = \psi(x, y)$, $\chi = z$, leading to the more familiar expressions $u_x = \frac{\partial \psi}{\partial y}$, $u_y = -\frac{\partial \psi}{\partial x}$, where ψ is recognized to be the streamfunction. The time of flight, τ, is defined simply as the travel time of a neutral tracer along the streamlines,

$$\tau(x, y, z) = \int \frac{\phi \, ds}{|\vec{u}|} \quad \text{.....} \tag{2.3}$$

Or, in a differential form as follows

$$\vec{u} \cdot \nabla \tau = \phi \quad \text{.....} \tag{2.4}$$

Streamline techniques are based upon a coordinate transformation from the physical space to the time of flight coordinate where all the streamlines can be treated as straight lines of varying lengths. This coordinate transformation is greatly facilitated by the fact that the Jacobian of the coordinate transformation assumes an extraordinarily simple form when using **Eq. 2.1** and **Eq. 2.4**:

$$\left\| \frac{\partial(\tau, \psi, \chi)}{\partial(x, y, z)} \right\| = \nabla \tau \cdot (\nabla \psi \times \nabla \chi) = \nabla \tau \cdot \vec{u} = \phi \, . \tag{2.5}$$

Starting from this expression, we have the following relationship between the physical space and the time of flight coordinates following the flow direction,

$$\phi \, dx \, dy \, dz = d\tau \, d\psi \, d\chi \, . \quad \text{.....} \tag{2.6}$$

It is now easy to see that the coordinate transformation also preserves the pore volume, which is an essential feature to preserve the material balance.

Spatial gradients along streamlines become a very simple form in the time of flight coordinates. Using the (τ, ψ, χ) coordinates, the gradient operator can be expressed as:

$$\nabla = (\nabla\tau)\frac{\partial}{\partial\tau} + (\nabla\psi)\frac{\partial}{\partial\psi} + (\nabla\chi)\frac{\partial}{\partial\chi} \text{ .....} \quad (2.7)$$

Because $\vec{u}$ is orthogonal to both $\nabla\psi$ and $\nabla\chi$,

$$\vec{u} \bullet \nabla = \phi\frac{\partial}{\partial\tau} \text{ .....} \quad (2.8)$$

The major advantage of the τ coordinate becomes evident when we consider the conservation equation for the water phase in two-phase incompressible flow, away from sources and sinks,

$$\phi\frac{\partial S_w}{\partial t} + \nabla \bullet (F_w\vec{u}) = 0 \text{ .....} \quad (2.9)$$

This expression can be expanded and transformed using the τ coordinate,

$$\frac{\partial S_w}{\partial t} + \frac{\partial F_w}{\partial\tau} = 0 \text{ .....} \quad (2.10)$$

After this coordinate transformation, we have decomposed the three dimensional fluid flow into a series of one dimensional (in τ) evolution equation for S_w along streamlines. This equation is just as valid in one, two and three dimensions, and for homogeneous and heterogeneous media. The τ transformation includes all of these effects. All that is required for implementation is the velocity field and the calculation of the line integral in **Eq. 2.3**.

2.2 Generalization to Compressible Flow

Compressibility generates a change in effective volume that will depend upon pressure change, specifically the $\frac{\partial P}{\partial t}$ term. If the pressure drops, then we expect the total volumetric flux from a cell to be positive. Thus, the divergence of the total flux no longer vanishes. This requires redefinition of the bi-streamfunctions to account for compressibility effects,

$$\rho\vec{u} = \nabla\psi \times \nabla\chi \quad \text{.....} \tag{2.11}$$

where we have introduced the 'effective density', ρ. For incompressible flow, ρ = 1. We can develop **Eq. 2.11** further by recognizing that $\rho\vec{u}$ now represents a conserved flux.[16]

$$\begin{aligned} 0 = \nabla \bullet (\nabla\psi \times \nabla\chi) &= \nabla \bullet (\rho\vec{u}) \\ &= \vec{u} \bullet \nabla\rho + \rho\nabla \bullet \vec{u} \\ &= \phi\frac{\partial\rho}{\partial\tau} + \rho\nabla \bullet \vec{u} \end{aligned} \quad \text{.....} \tag{2.12}$$

Eq. 2.12 can be reduced to an ordinary differential equation that can be integrated to obtain ρ along streamlines. This becomes apparent when we recognize that $\nabla \bullet \vec{u}$ within each gridcell is a constant. In fact, the computing of ρ can be carried out in conjunction with the streamline tracing using the algorithm of Pollock.[17] The Pollock algorithm assumes that the cell velocities vary linearly in the respective directions, that is,

$$\begin{aligned} u_x &= u_{x1} + c_x(x - x_1) \\ u_y &= u_{y1} + c_y(y - y_1) \\ u_z &= u_{z1} + c_z(z - z_1) \end{aligned} \quad \text{.....} \tag{2.13}$$

where the coefficients, *C*, depend on the difference of Darcy velocities on the grid block faces (**Fig. 2.1**),

$$\begin{aligned} c_x &= (u_{x2} - u_{x1})/\Delta x \\ c_y &= (u_{y2} - u_{y1})/\Delta y \\ c_z &= (u_{z2} - u_{z1})/\Delta z \end{aligned} \quad \text{.....} \tag{2.14}$$

From **Eq. 2.13**, it follows that

$$\nabla \bullet \vec{u} = \sum_{j=1}^{3} c_j = c_x + c_y + c_z \quad \text{.....} \tag{2.15}$$

Eq. 2.12 can now be integrated:

$$\rho = \rho_0 e^{-\left(\sum_{j=1}^{3} c_j\right)\left(\frac{\tau}{\phi}\right)} \quad \text{.....} \tag{2.16}$$

The value for this effective density can be traced along each streamline from the injectors where $\rho_0 = 1$ and where the initial volumetric flux q_o, is assigned to a streamline. Along the streamline, the volumetric flux will now be given by $q = q_o / \rho$. Instead of working with an effective density, it is as easy to work with this volumetric flux

$$q = q_0 e^{\left(\sum_{j=1}^{3} c_j\right)\left(\frac{\tau}{\phi}\right)} \quad \text{.....} \tag{2.17}$$

This equation provides a definition of the volumetric flux along any streamline, consistent with the velocity field.

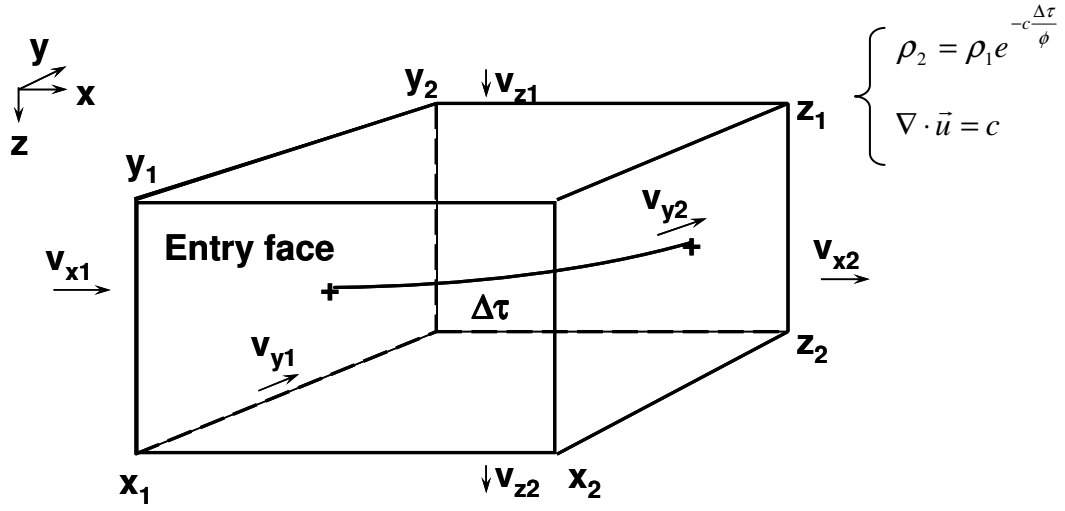

Figure 2.1— Ponting algorithm with compressible fluid.

It is interesting to note that compressibility does not generate any transverse flux corrections. This is counter-intuitive at first, until one realizes that the bi-streamfunctions of **Eq. 2.11** already include the effects of compressibility on the traces of the streamlines. However, volumetric flux is not conserved on these lines (or tubes); the volumetric flux that enters a tube or is assigned to a line will be modified along its length, according to **Eq. 2.17**.

For compressible flow, another modification that needs to be done is the Jacobian of the transformation from (x, y, z) to (τ, ψ, χ), to modify the relationship of volumes. Now we have

$$\left\| \frac{\partial(\tau, \psi, \chi)}{\partial(x, y, z)} \right\| = \left| (\nabla \psi \times \nabla \chi) \bullet \nabla \tau \right| = \left| \rho \vec{u} \bullet \nabla \tau \right| = \rho \phi \tag{2.18}$$

In terms of volume we have.

$$\phi dx dy dz = \frac{1}{\rho} d\tau d\psi d\chi \text{ .....} \tag{2.19}$$

In integral form,

$$Q = \vec{u} \bullet \delta \vec{a} = \iint q \, d\psi \, d\chi \text{ .....} \tag{2.20}$$

because the volumetric flux now depends upon the position along the streamline. No other aspects of the streamline time of flight formulation need to be modified for convective flux. The coordinate transformation in **Eq. 2.19** can be used to transform multidimensional saturation equation to a series of 1-D saturation equations along streamlines using time of flight as the spatial coordinate. This is identical to the incompressible case. However, the compressibility effects will result in a source/sink term in the 1-D saturation equation to account for fluid expansion and compression along streamlines. The details of the derivation and solution of the saturation equations for compressible flow are discussed in the next section for two and three-phase black oil simulation.

2.3 Illustration of the Rigorous Compressible Streamline Formulation

We now illustrate the calculations using waterflood in a homogeneous ¼-spot pattern under black oil conditions and compare the results with the incompressible streamline formulation**. Fig. 2.2a** shows the pressure distribution for a two-phase black oil case computed using finite-difference. The initial reservoir pressure was set at 3000 psi and the producer is bottomhole pressure constrained at 1000 psi. Both water and oil are treated as compressible fluids summarized in **TABLE 2.1**, although the oil compressibility is kept somewhat higher than usual to have a pronounced effect. The bubble point pressure was set sufficiently low to ensure undersaturated conditions and no free gas for this example. The three-phase case will be considered later.

TABLE 2.1—FLUID PROPERTIES OF WATER AND OIL

	Compressibility [1/psi]	Viscosity [cp]
Water	1.00E-06	1.0
Oil	4.60E-04	2.0

The velocity field obtained from the pressure distribution is used to trace streamlines and compute time of flight using the Pollock algorithm [17] as in the incompressible case. Note that the Pollock algorithm is sufficiently general and is not limited to incompressible flow. However, unlike incompressible flow, streamlines can now originate and terminate anywhere in the domain. While tracing streamlines, we also compute the divergence of flux at each grid cell using **Eq. 2.15**. The divergence of flux is shown in **Fig. 2.2b**. The streamline time of flight for this ¼ five-spot example is shown in **Fig. 2.2c** at t=200 days.

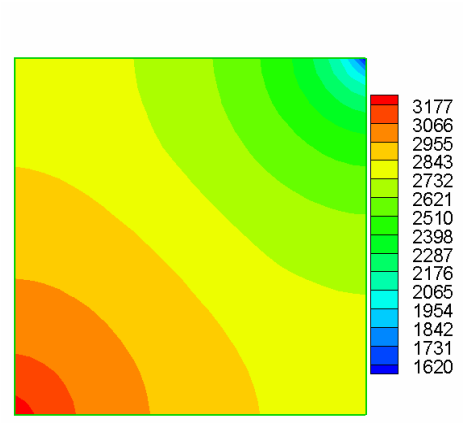

(a) Pressure distribution

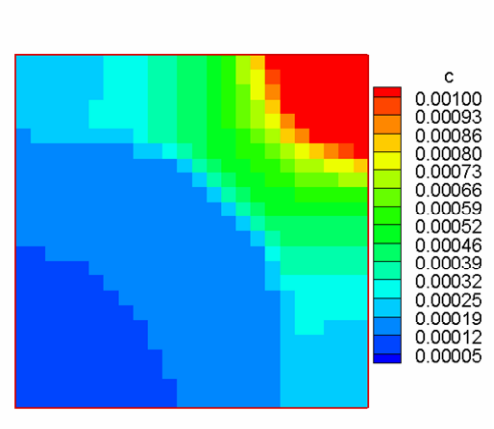

(b) Divergence of flux

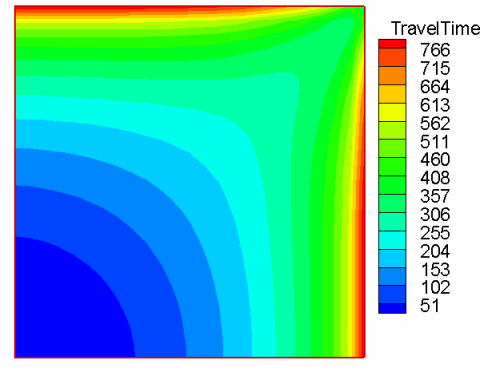

(c) Streamline time of flight

Figure 2.2— Contour plots of waterflood in a ¼ spot pattern.

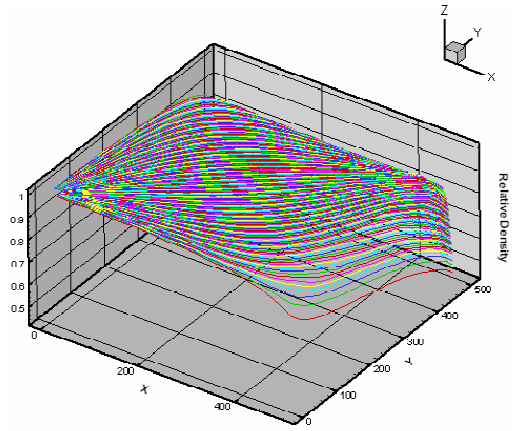

(a) Tracing relative density along streamline

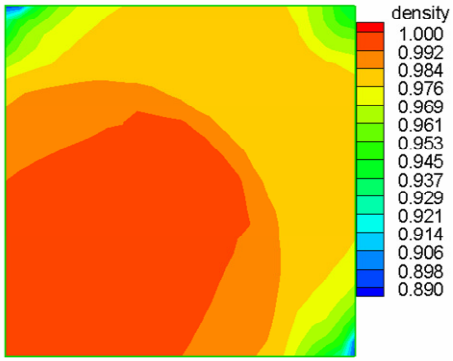

(b) 'local'

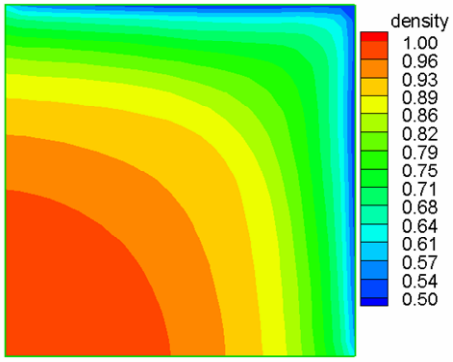

(c) 'accumulated'

Figure 2.3— Contour plots of changes in relative density.

Next we calculate the effective densities along streamlines using **Eq. 2.16** and show in **Fig. 2.3.a**. A contour of the 'local' changes in effective density ($\Delta\rho$ for each grid cell) is shown **Fig. 2.3b**. A value of less than unity indicates expansion of the fluid in the grid cell and vice versa. Note that the changes in effective density are a function of fluid compressibility, porosity and

time of flight. The relatively low values at the stagnant corners reflect the large cell time of flight there.

The accumulated effective densities along streamlines are contoured in **Fig. 2.3c** and resemble the time of flight distribution. In fact, based on **Eq. 2.19**, we can view the relative densities as scale factors for the time of flight, 'accelerating' or 'retarding' the particle transport along streamlines. The oil rate at the producing well for the compressible streamline calculations is shown in **Fig. 2.4**. For validation purposes, we have also shown the results from finite difference simulation. There is very good agreement between streamline and finite difference calculations. Fluid compressibility of oil gives high production rate initially, however the injecting water support is not high enough to maintain the high oil production rate and causing the smooth reduction of production rate. The rapid reduction is because of the water breakthrough. Finally, to demonstrate the effects of fluid compressibility, we have also superimposed the results from incompressible streamline formulation. Clearly, the compressibility effects are too large to be ignored for this case. Because of incompressibility of the reservoir fluid, injecting constant surface rate of water is replacing the reservoir oil with constant rate even though the producing well has bottom hole pressure constraints, and the rapid reduction of oil production rate is indicating the water breakthrough.

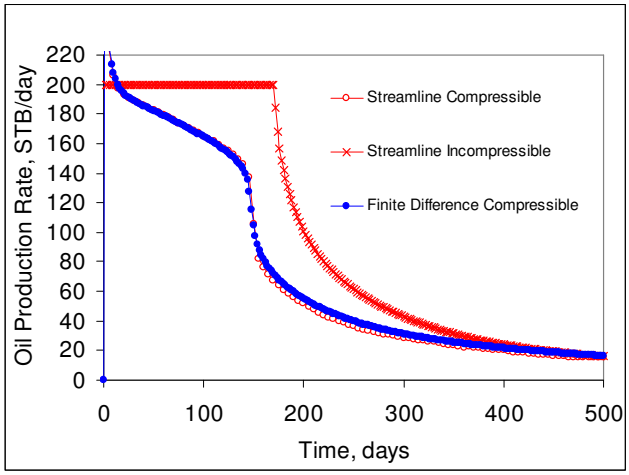

Figure 2.4— Impact of compressibility in oil production rate.

The example discussed so far involves mostly fluid expansion as the pressure was below the initial pressure throughout the reservoir except in the vicinity of the injection well. In next example, we increased bottomhole pressure to 2500 psi and kept other parameters. The reservoir

pressure for the most part is now above the initial pressure and fluid is under compression throughout the reservoir. This is also indicated by the cell values of divergence of flux which are all negative as shown in **Fig. 2.5**. **Fig. 2.6** shows the tracing of the effective density along the streamlines. The contour of the effective density is shown in **Fig. 2.7**. Notice that unlike the previous case, the effective densities are now greater than unity everywhere reflecting fluid compression along streamlines. As before, the effective density distribution is significantly impacted by the time of flight.

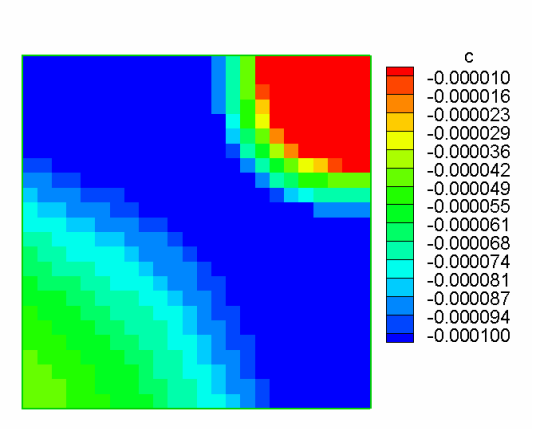

Figure 2.5— Cell value of *C* for compressible case.

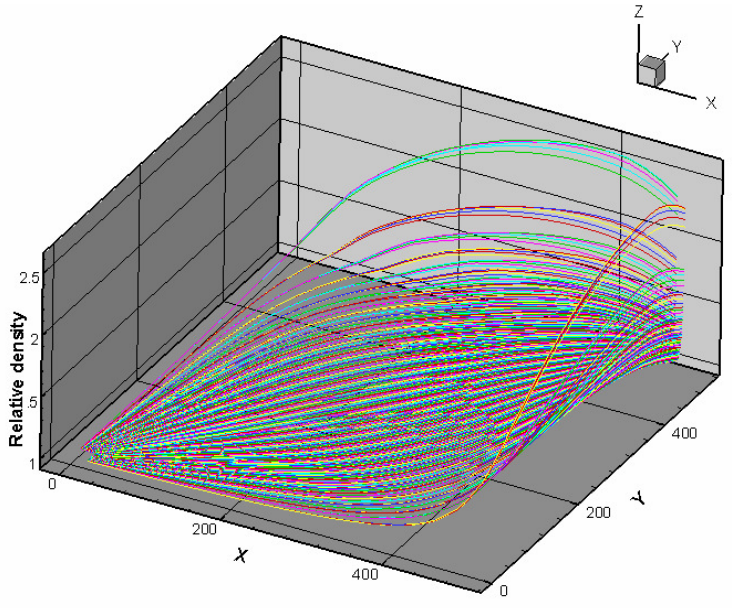

Figure 2.6—Tracing density along streamline.

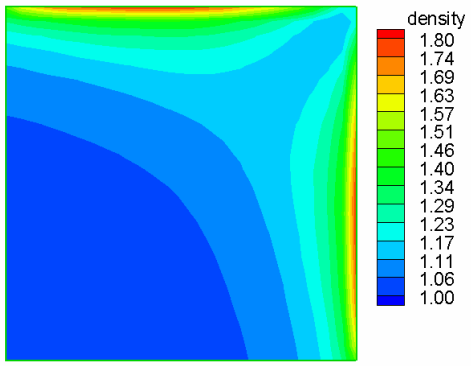

Figure 2.7—Contour plot of relative density.

Fig. 2.8 shows the oil production rate vs. time using the compressible streamline formulation and a commercial finite difference simulator. Notice the dramatically different behavior for this example compared to the previous case. Clearly, our proposed formulation adequately captures the effects of fluid expansion and compression. For comparison purposes, we also show the results from a commercial streamline simulator using black oil properties. The improvements resulting from our new formulation is quite obvious here.

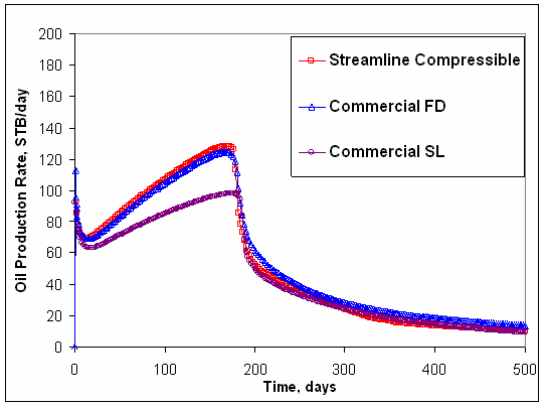

Figure 2.8—Oil production rate vs. time.

CHAPTER III

TWO AND THREE – PHASE BLACK OIL SIMULATION*

This chapter presents the extension of compressible streamline formulation to two and three – phase black oil simulation. Conventional streamline has applied in many waterflooding cases because inherent incompressible assumptions are true in these situations. However, most of the reservoirs have some degree of compressibility and black oil fluid representation is widely used for reservoirs which do not have so complex fluid representations because of computational advantages compared to compositional model which can handle even more complex fluid representations. Thus, we first show two and three – phase black oil streamline formulations. Then we also introduce time-step selection for pressure update in compressible streamline simulation by using correction CFL approach. Since we have gas phase in our model, we also show the operator splitting approach to capture gravity segregation problems.

Finally, the power and computational efficiency of our approach are demonstrated by applications to synthetic and field examples. The synthetic examples include a 2-D homogeneous ¼ spot case and also 2-D cross sectional case for gravity segregation problems. And the field example is from the Goldsmith San Andres Unit (GSAU) in West Texas and includes multiple patterns with 11 injectors and 31 producers. All of our examples show the rigorousness of our compressible streamline formulation into two and three - phase black oil model in terms of accuracy and computational efficiency.

3.1 Streamline Saturation Equation for Two and Three - Phase Black Oil

3.1.1 Streamline Saturation Equation for Two – Phase Black Oil

The water mass conservation equation for two-phase black oil case is given by,

---

* Part of this chapter is reprinted with permission from "A Rigorous Compressible Streamline Formulation for Two and Three-Phase Black Oil Simulation," by Hao Cheng, Ichiro Osako, Akhil Datta-Gupta, and Michael J. King, paper SPE 96866 presented at the 2005 SPE Annual Technical Conference and Exhibition, Dallas, TX, October 9-12, Copyright 2005 by the Society of Petroleum Engineers.

$$\phi\frac{\partial}{\partial t}\left(\frac{S_w}{B_w}\right)+\nabla\bullet\left(\frac{F_w\vec{u}}{B_w}\right)=0 \text{ .....} \quad (3.1)$$

where, B_w is formation volume factor of water, and F_w is fractional flow of water.
Expanding the divergence operator we get,

$$\phi\frac{\partial}{\partial t}\left(\frac{S_w}{B_w}\right)+\frac{F_w}{B_w}\nabla\bullet\vec{u}+\vec{u}\bullet\nabla\left(\frac{F_w}{B_w}\right)=0 \text{ .....} \quad (3.2)$$

Now, transforming to streamline time of flight coordinates using, $\vec{u}\bullet\nabla=\phi\frac{\partial}{\partial\tau}$, and setting $\nabla\cdot\vec{u}=\sum_{j=1}^{3}c_j=c$, we obtain

$$\frac{\partial}{\partial t}\left(\frac{S_w}{B_w}\right)+\frac{\partial}{\partial\tau}\left(\frac{F_w}{B_w}\right)=-\frac{c}{\phi}\frac{F_w}{B_w} \text{ .....} \quad (3.3)$$

It is now clear that compressibility effects act as source/sink terms along streamlines to account for fluid expansion/compression. Note that c is spatially varying along the streamline and can be obtained by mapping divergence of flux computed for each grid cell onto the streamline. For incompressible flow, $c=0$ everywhere and the right hand term vanishes. We can re-write **Eq. 3. 3** in terms of the effective density along streamline using the following relation,

$$\frac{c}{\phi}=-\frac{1}{\rho}\frac{\partial\rho}{\partial\tau} \text{ .....} \quad (3.4)$$

Eq. 3.4 follows directly from **Eq. 2.16.** The saturation equation can now be expressed as,

$$\frac{\partial}{\partial t}\left(\frac{S_w}{B_w}\right)+\frac{\partial}{\partial\tau}\left(\frac{F_w}{B_w}\right)=\frac{1}{\rho}\frac{F_w}{B_w}\frac{\partial\rho}{\partial\tau} \text{ .....} \quad (3.5)$$

For numerical solution along streamline we can use either **Eq. 3.3** or **Eq. 3. 5** because both c and ρ are available along streamlines. Discretizing **Eq. 3.3**, we get,

$$\frac{1}{\Delta t}\left(\frac{S_w}{B_w}\bigg|^{n+1} - \frac{S_w}{B_w}\bigg|^{n}\right) + \frac{1}{\Delta\tau}\left(\frac{F_w}{B_w}\bigg|^{n}_{i-1/2} - \frac{F_w}{B_w}\bigg|^{n}_{i+1/2}\right) = -\frac{c}{\phi}\frac{F_w}{B_w}\bigg|^{n}_{i} \tag{3.6}$$

where the interblock quantities need to be approximated appropriately as in conventional finite difference simulation. We use upstream weighting for F_w and midpoint weighting for B_w.

For compressible flow, the pressure field needs to be updated more often compared to incompressible flow. Also, the saturation along streamlines will need to be mapped back onto the finite difference grid as in the incompressible streamline formulation. However, for compressible flow, we need to utilize **Eq. 2.19** whereby the effective density, the flow rate and the time-of-flight information are used to incorporate cross-streamline effects and remapping of saturations. Note that along any streamline, we must satisfy the mass balance constraint,

$$\rho_i q_i = \rho_j q_j \text{ .....} \tag{3.7}$$

where *i* and *j* are two arbitrary nodes along the streamline. Because $\rho = 1$ at the injector, the flow rate at any position along the streamline can be related to the assigned rate at the injector, q_0 as follows,

$$q_i = q_0 \frac{1}{\rho_i} \text{ .....} \tag{3.8}$$

While mapping saturations from streamline segments to a grid-block, we need to take into account the variation in flow rates along streamlines. The average saturation in a grid block can be calculated by weighting the saturation, local flow rate and time of flight of each streamline segment passing through the grid block as follows

$$\bar{S}_w = \frac{\sum_{\psi_i} (S_w)_i \cdot q_i \cdot \Delta\tau_i}{\sum_{\psi_i} q_i \cdot \Delta\tau_i} \text{ .....} \tag{3.9}$$

3.1.2 Streamline Saturation Equation for Three – Phase Black Oil

We now extend the concepts developed for two-phase black oil simulation to three-phase flow conditions. The water saturation equation remains unchanged from the two-phase case. In addition, we now have the mass conservation equation for gas as follows,

$$\phi \frac{\partial}{\partial t}\left(\frac{S_g}{B_g}+\frac{S_o R_s}{B_o}\right)+\nabla \bullet \left(\vec{u}\frac{F_g}{B_g}+\vec{u}\frac{F_o R_s}{B_o}\right)=0 \cdots\cdots \tag{3.10}$$

where, R_s is solution gas oil ratio. Following the same procedure discussed for two-phase black oil simulation, we obtain the following equations for gas saturation along streamlines,

$$\frac{\partial}{\partial t}\left(\frac{S_g}{B_g}+\frac{S_o R_s}{B_o}\right)+\frac{\partial}{\partial \tau}\left(\frac{F_g}{B_g}+\frac{F_o R_s}{B_o}\right)=-\left(\frac{F_g}{B_g}+\frac{F_o R_s}{B_o}\right)\frac{c}{\phi} \tag{3.11}$$

Or,

$$\frac{\partial}{\partial t}\left(\frac{S_g}{B_g}+\frac{S_o R_s}{B_o}\right)+\frac{\partial}{\partial \tau}\left(\frac{F_g}{B_g}+\frac{F_o R_s}{B_o}\right)=\left(\frac{F_g}{B_g}+\frac{F_o R_s}{B_o}\right)\frac{1}{\rho}\frac{\partial \rho}{\partial \tau}$$

3.1.3 Operator Splitting Technique for Gravity Segregation Problems

In streamline simulation, operator splitting method has been used to apply 1-D front tracking schemes to multidimensional problems and also for including gravity by Bratvedt *et al.*[10, 24] By including gravity the fractional flow is,

$$u_w=\frac{\lambda_w}{\lambda_t}\vec{u}+\frac{g}{\vec{u}}\frac{\lambda_w}{\lambda_t}\left\{\lambda_o\left(\rho_o-\rho_w\right)+\lambda_g\left(\rho_g-\rho_w\right)\right\}=\vec{u}F_w+G_w \tag{3.12}$$

At this point, it is important to notice the distinction in the symbols, f_w and F_w. And G_w is given by,

$$G=\frac{g}{\vec{u}}\frac{\lambda_w}{\lambda_t}\left\{\lambda_o\left(\rho_o-\rho_w\right)+\lambda_g\left(\rho_g-\rho_w\right)\right\}$$

Applying **Eq. 3.12**. into **Eq. 3.10**,

$$\phi\frac{\partial}{\partial t}\left(\frac{S_w}{B_w}\right)+\nabla\cdot\left(\frac{u_w}{B_w}\right)=\phi\frac{\partial}{\partial t}\left(\frac{S_w}{B_w}\right)+\nabla\cdot\left(\vec{u}\,\frac{F_w}{B_w}+\frac{G_w}{B_w}\right)=0 \tag{3.13}$$

Expanding the divergence term,

$$\nabla\cdot\left(\vec{u}\,\frac{F_w}{B_w}+\frac{G_w}{B_w}\right)=\frac{F_w}{B_w}\nabla\cdot\vec{u}+\vec{u}\cdot\nabla\left(\frac{F_w}{B_w}\right)+\nabla\cdot\left(\frac{G_w}{B_w}\right) \tag{3.14}$$

And applying the time of flight coordinate, the conservation equation will be

$$\frac{\partial}{\partial t}\left(\frac{S_w}{B_w}\right)+\frac{F_w}{\phi B_w}\nabla\cdot\vec{u}+\frac{\partial}{\partial\tau}\left(\frac{F_w}{B_w}\right)+\frac{1}{\phi}\nabla\cdot\left(\frac{G_w}{B_w}\right)=0 \tag{3.15}$$

We can not solve the conservation equation along streamlines because the gravity term does not follow the streamline direction. Operator splitting allows us to solve the equation by starting with the convective term to account for convection along the streamline and then moving to the gravity term accounting for density difference. Thus we split the conservation equation into two equations as

$$\frac{\partial}{\partial t}\left(\frac{S_{w1}}{B_w}\right)+\frac{\partial}{\partial\tau}\left(\frac{F_w}{B_w}\right)=-\frac{F_w}{\phi B_w}\nabla\cdot\vec{u}\quad(\nabla\cdot\vec{u}=c)\cdot\cdot \tag{3.16}$$

$$\frac{\partial}{\partial t}\left(\frac{S_{w2}}{B_w}\right)+\frac{1}{\phi}\nabla\cdot\left(\frac{G_w}{B_w}\right)=0\ \cdots\cdots\cdots\cdots\cdots\cdots\cdots\cdots \tag{3.17}$$

First equation is solved along the streamline as in the conventional streamline simulation. Once the convection part of saturation update has been done along all streamlines, saturation data is mapped back onto the Cartesian grid blocks and then a second equation is solved on the Cartesian grid blocks. While solving **Eq. 3.17**, one has to be careful about the upstream treatment of the phase. Following the approach of Sammon [19], **Eq. 3.17** is discretized to

$$S_{w2}^{n+1}=B_w^{n+1}\frac{S_{w1}}{B_w}\bigg|^n-\frac{B_w^{n+1}\Delta t}{\phi\Delta z}\left(\frac{G_w(S_{w1})}{B_w}\bigg|^n_{k+1/2}-\frac{G_w(S_{w1})}{B_w}\bigg|^n_{k-1/2}\right)=0 \tag{3.18}$$

where, $B^n_{w,k+1/2}=\frac{1}{2}\left(B^n_{w,k+1}+B^n_{w,k}\right)$, $B^n_{w,k-1/2}=\frac{1}{2}\left(B^n_{w,k-1}+B^n_{w,k}\right)$,

$$G_w(S_{w1})\big|^n_{k+1/2}=\frac{\lambda_{w,k}g\{(\rho_o-\rho_w)\lambda_{o,k+1}+(\rho_g-\rho_w)\lambda_{g,k+1}\}}{\lambda_{o,k+1}+\lambda_{g,k+1}+\lambda_{w,k}},$$

$$G_w(S_{w1})\Big|_{k-1/2}^{n} = \frac{\lambda_{w,k-1} g\{(\rho_o - \rho_w)\lambda_{o,k} + (\rho_g - \rho_w)\lambda_{g,k}\}}{\lambda_{o,k} + \lambda_{g,k} + \lambda_{w,k-1}}$$

3.1.4 Synthetic Examples

In this section we present simulation results for three-phase flow using the compressible streamline formulation since our two-phase synthetic examples are shown in the illustration of the method. First, we simulated water injection in a ¼ five-spot pattern with three-phase flow. A homogeneous permeability model represented by 25×25 grid cells was used. The initial solution GOR is 1.27 Mscf/STB. Initial reservoir pressure is 3005 psi and the initial gas saturation is set at 0.2 everywhere. The producer is bottomhole pressure constrained at 2500 psi, and the injector is rate constrained at 250 B/d. **TABLE 3.1** and **3.2** summarize fluid properties of oil and gas. Water properties are remained same as two-phase example. A pressure update time step of 2 days was used in these simulations. **Figs. 3.1** show the oil, gas and water production rates, respectively. An explicit finite difference solution was used for 1-D saturation transport along streamlines. The oil rate starts with a relatively large value because of the initial pressure drawdown. However, as the gas saturation builds up, the oil rate declines and then rises again as the oil bank is produced. For comparison purposes, we have superimposed the results from finite difference simulation. The agreement is, indeed, very close**. Fig. 3.2** compares the water and gas saturation profiles from streamline and finite-difference simulation at 1750 days. Again, the saturation distributions are in good agreement.

TABLE 3.1—FLUID PROPERTIES OF OIL

Rs [Mscf/STB]	Pb [psi]	Bo [RB/STB]	Viscosity [cp]
0.001	14.7	1.062	1.04
0.11	264.7	1.15	0.915
0.219	514.7	1.207	0.829
0.433	1014.7	1.324	0.732
0.643	1514.7	1.411	0.663
0.862	2014.7	1.514	0.613
1.057	2514.7	1.605	0.551
1.27	3000	1.695	0.51
1.27	3514.7	1.671	0.549
1.27	9014.7	1.579	0.74

TABLE 3.2—FLUID PROPERTIES OF GAS

Pg [psi]	Bg [RB/Mscf]	Viscosity [cp]
14.7	166.666	0.008
264.7	12.093	0.0096
514.7	6.274	0.0112
1014.7	3.197	0.014
2014.7	1.614	0.0189
2514.7	1.294	0.0208
3014.7	1.08	0.0228
4014.7	0.811	0.0268
5014.7	0.649	0.0309
9014.7	0.386	0.047

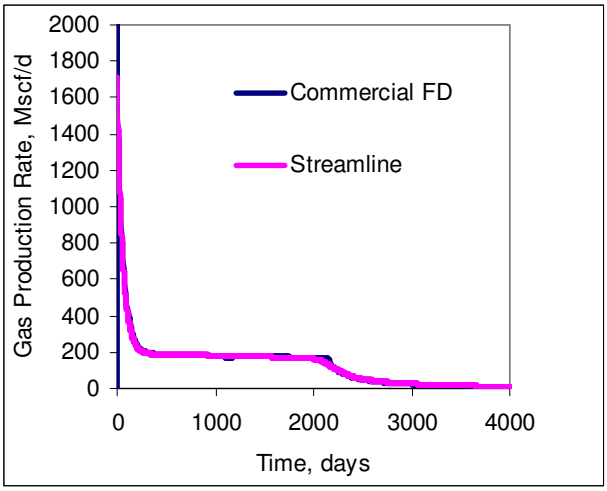

(a) Gas production rate

Figure 3.1—Production vs. time for three phase flow and comparison with finite difference.

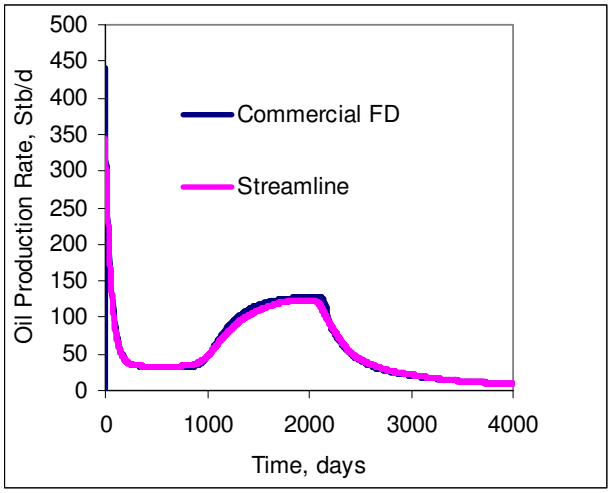

(b) Oil production rate

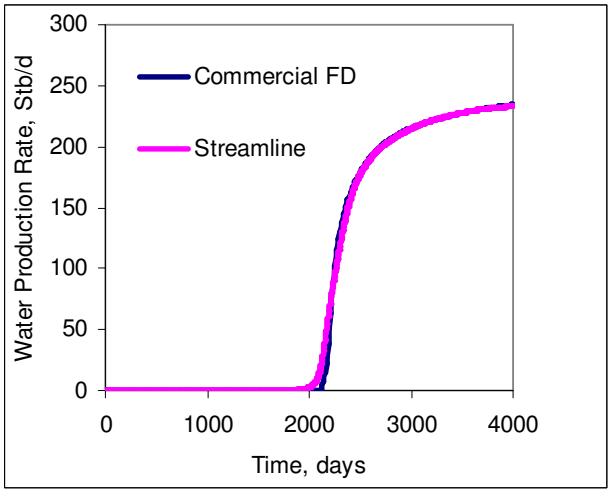

(c) Water production rate

Figure 3.1—Continued.

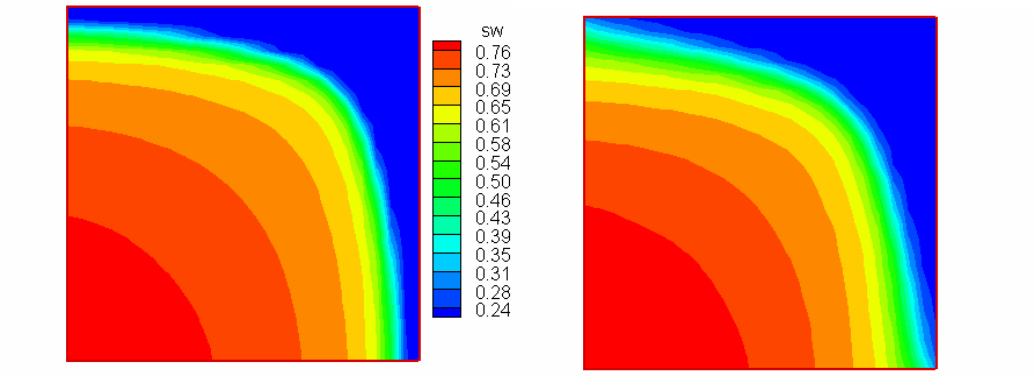

(a) Water saturation

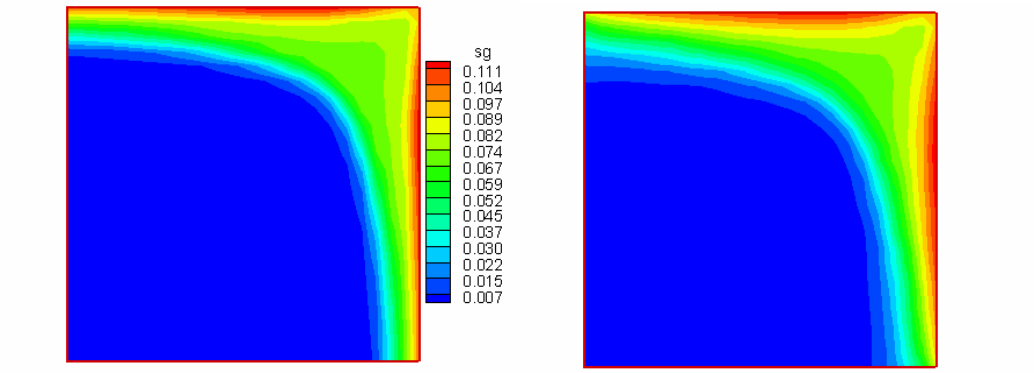

(b) Gas saturation

Figure 3.2—Water and gas saturation distribution: finite difference (left) vs. streamline (right).

Second example is 2-D cross sectional case to demonstrate the gravity segregation problems. A homogeneous permeability model represented by 25×1×25 grid cells was used. Initial reservoir condition and fluid properties are almost same as in the last example. The producer is bottomhole pressure constrained at 2500 psi in right side of the reservoir, and the injector is rate constrained at 800 B/d in the left side of reservoir. Both injection and production wells are perforated through all layers. A pressure update time step of 2 days was used in these simulations. Gas saturation profiles of finite difference and our streamline simulation without gravity option are compared in **Fig. 3.3**. As we see, we could clearly see there is no gravity segregation in our streamline simulation. However, by including the gravity option, as we see in **Fig. 3.4** showing the comparison of finite difference and our streamline with gravity option, we can capture the gravity segregation well.

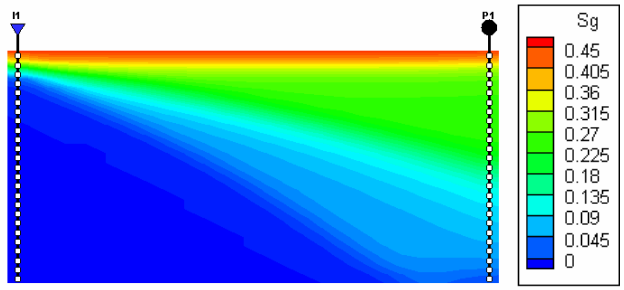

Figure 3.3—Gas saturation distribution: finite difference.

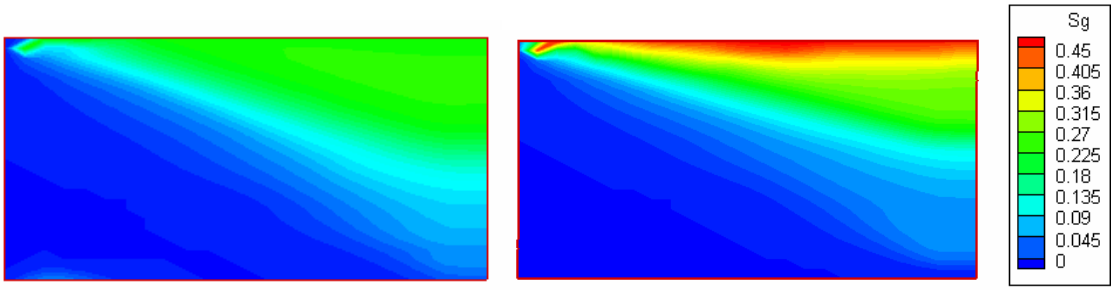

(a) without gravity segregation (b) with gravity segregation

Figure 3.4—Gas saturation distribution: streamline.

3.1.5 Field Example

We have applied the compressible streamline formulation to perform black oil simulation of waterflooding in a CO_2 pilot project area in the Goldsmith San Andres Unit (GSAU), a dolomite formation located in west Texas.[20] The pilot area consists of nine inverted 5-spot patterns covering around 320 acres with an average thickness of 100 ft, We have over 50 years of production history prior to CO_2 project initiation in Dec. 1996. **Fig. 3.5** shows the CO_2 pilot project site in the GSAU. We performed streamline simulation for 20 years of waterflood prior to the initiation of CO_2 injection.

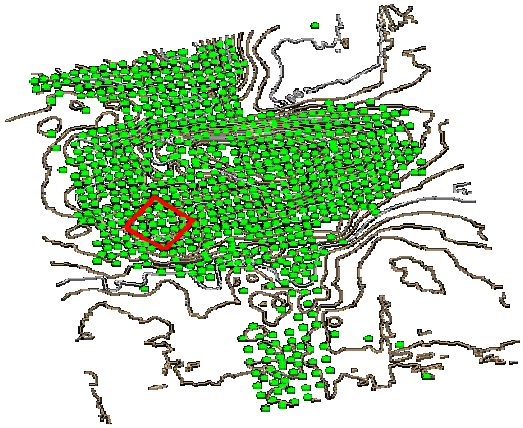

Figure 3.5— Goldsmith field CO2 pilot area (shown within the box).

Because of the practical difficulties in obtaining the correct boundary conditions for the pilot area, extra wells located outside the pilot area were included in this study. The extended study area consists of 11 water injectors and 31 producers. The study area is discretized into 58x53x10 mesh or a total of 30,740 grid cells. The porosity field, shown in **Fig. 3.6**, is obtained by a Sequential Gaussian Simulation using the well log and seismic data. The permeability field is generated via a cloud transform based on the porosity-permeability relationship and shown in **Fig. 3.7**.

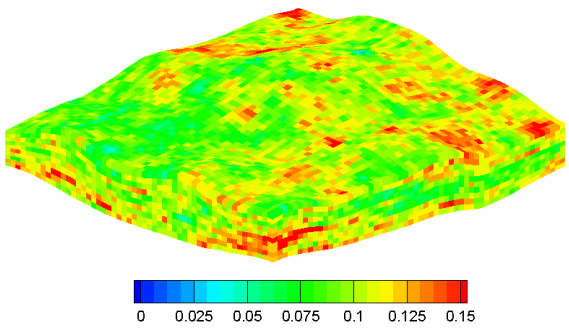

Figure 3.6— Porosity distribution.

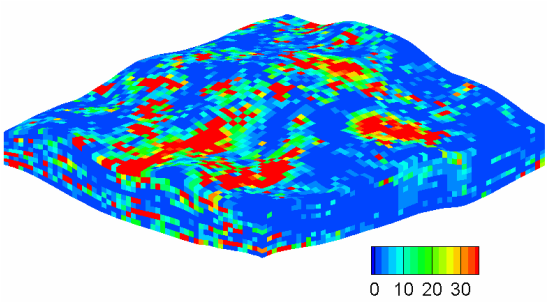

Figure 3.7— Permeability distribution.

We compare the water cut and oil production rates in all the producing wells using our proposed streamline formulation and a commercial finite difference simulator for a total 7800 days. At the beginning of the waterflood, water saturation was 0.225. Both water and oil are treated as compressible fluids with live oil PVT properties summarized in **TABLE 3.3**. The reservoir pressure was kept above the bubble point pressure throughout the simulation. No capillary pressure was included in these simulations. The simulation results are shown in **Fig. 3.8** for a selected number of wells. Our proposed formulation closely follows the results from the finite difference simulator.

TABLE 3.3—FLUID PROPERTIES OF WATER AND OIL

	Compressibility [1/psi]	Viscosity [cp]
water	1.00E-06	0.79
oil	4.60E-06	0.4747

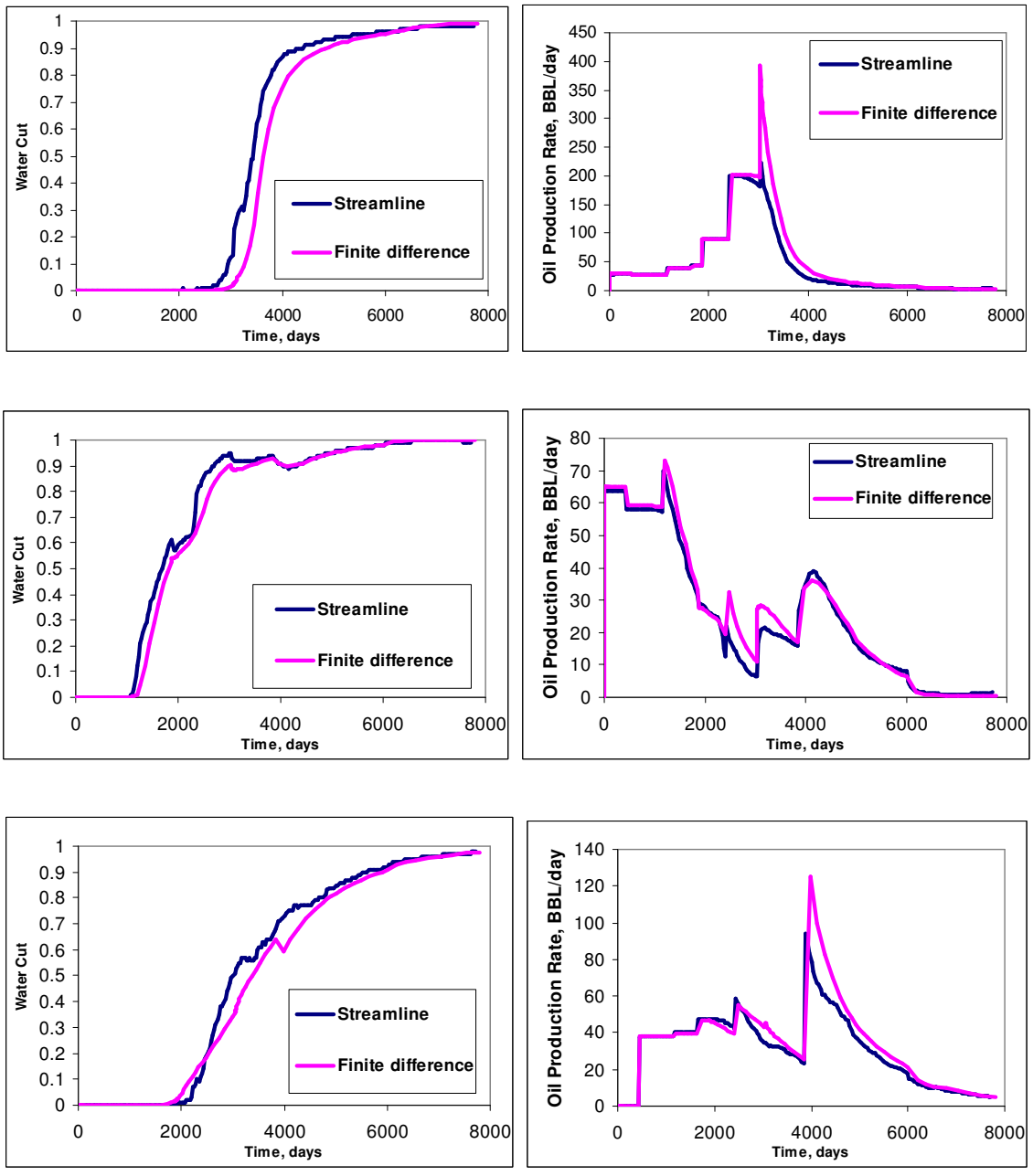

Figure 3.8— Comparison with a commercial finite-difference simulator for a few selected wells.

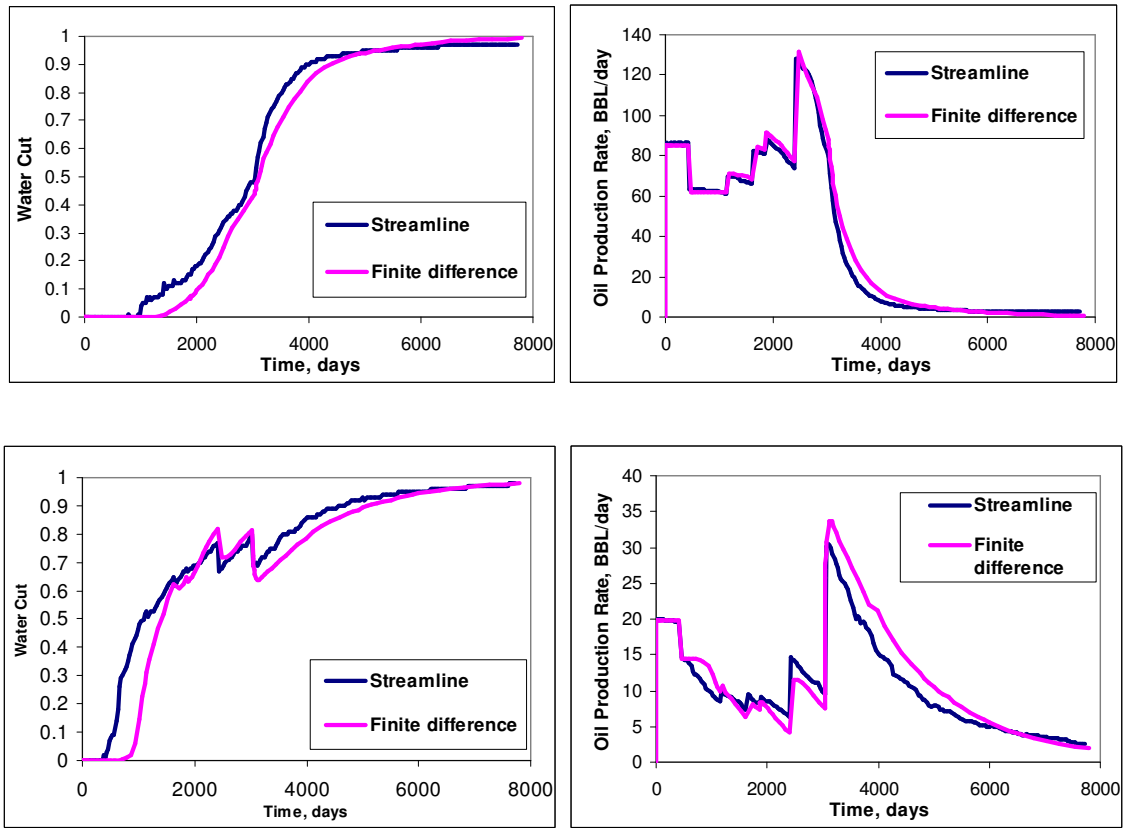

Figure 3.8— Continued.

Our primary emphasis in this paper has been the new formulation rather than the computational aspects. As in the incompressible case, the compressible streamline simulation is likely to be most advantageous for flow simulation through high resolution geologic models and very large simulation models. However, as we discuss in the next section, the speed up factor will be less compared to the incompressible case. This computational advantage will mainly arise from two reasons. First, the streamline approach will require fewer pressure solutions. This is particularly the case for moderate to adverse mobility ratio displacements.[21] Second, with our proposed compressible formulation the solution of the 1-D saturation equations is still decoupled from the underlying grid, thus allowing for larger time steps. To elaborate on these points, in **TABLE 3.4** we have compared the number of pressure solutions for streamline and finite difference simulation for all the cases presented here. For the finite difference simulation, we have attempted to optimize the time step size by selecting the automatic time step selection option in the commercial simulator. However, there could still be further scope for optimization.

So, these numbers should be treated as approximate. Nevertheless, these results appear to be consistent with the CFL calculations shown in the next section. From these results, we can see that for the two phase compressible cases, the stable time step size for streamline simulation is almost ten times larger than that of the finite difference simulator. However, this computational advantage is likely to diminish for three phase cases as indicated in **TABLE 3.4**.

TABLE 3.4—NUMBER OF PRESSURE UPDATES

Case \ Simulation	Streamline	Finite Difference
Two-Phase	25	465
Three-Phase	400	941
Field	229	2367

3.2 Stability Consideration and Pressure Time Selection

An obvious question is how to select the time step for pressure updates during compressible streamline simulation. Intuitively, we know that compressible flow will require more frequent pressure recalculations. But is there a stability criterion that we could use for pressure time step selection? Osako *et al.*[21] addressed this issue in the context of incompressible streamline simulation. In this section we show that the formulation is sufficiently general and the same logic applies for compressible flow. Following Osako *et al.*,[21] we can use operator splitting to rewrite **Eq. 3.2** in a predictor-corrector mode as follows,

$$\frac{\partial}{\partial t}\left(\frac{S_w}{B_w}\right)+\frac{\partial}{\partial \tau}\left(\frac{F_w}{B_w}\right)=-\frac{c}{\phi}\frac{F_w}{B_w}\cdot \quad \text{(3.19a)}$$

$$\phi\frac{\partial}{\partial t}\left(\frac{S_w}{B_w}\right)+\left(\vec{u}-\vec{u}_0\right)\cdot\nabla\left(\frac{F_w}{B_w}\right)=0\cdot \quad \text{(3.19b)}$$

where $\vec{u}_0$ represents the 'initial' velocity distribution (at the beginning of a time step) used to generate the streamline and compute the time of flight in **Eq. 3.19a** and $\vec{u}$ represents the 'instantaneous' velocity. Within the operator splitting approximation, this pair of equations is equivalent to the original three dimensional flow equation. The first equation is the usual streamline evolution equation with the source term to include compressibility effects. The second equation includes any and all unsteady state effects, whether transverse or longitudinal, those are usually neglected in the streamline formulation. In fact, we can solve the corrector

equation, **Eq. 3.19b,** at the end of each time step using finite difference methods to update the streamline-derived saturations. However, Osako *et al.*[21] pointed out that the main utility of this corrector equation is to define a 'correction' CFL (Courant-Fredrich-Levy) [22] number for determining the stable time step for pressure updating.

Based on the corrector equation and following the logic of Osako *et al.*,[21] the discrete CFL number for the compressible flow will be given by,

$$CFL = \frac{\Delta t}{PV} \sum_{Inflow\ Faces} \left((\vec{u}_f - \vec{u}_0) \bullet \vec{n}_f \cdot \underset{S_{wf}}{Max} \left(\frac{[F_w]}{[S_w]} \right) \right) \cdot \cdot \tag{3.20}$$

The summation is only taken over the inflow faces, e.g., $\vec{n}_f$ is inwardly directed cell face area, and $(\vec{u}_f - \vec{u}_0) \bullet \vec{n}_f$ must be positive. As usual, the stable time step will be given by the condition, $CFL \le 1.$ Note that the CFL equation for compressible flow is identical to that for incompressible flow. Is the magnitude also the same? The answer is obviously "no". Because of the compressibility effects, fluid velocities will change and so will the CFL number.

To illustrate the impact of compressibility on CFL numbers, we again examine waterflood in a ¼ five-spot pattern. We use an end point mobility ratio of 0.5 and summarize in **TABLE 3.5** because typically favorable mobility ratios are more challenging for streamline simulation.[23] To start with, we examine an incompressible case. **Fig. 3.9** shows the oil rate for various pressure update time steps and the corresponding *CFL* numbers. For comparison purposes, we have also shown the results from a finite difference simulation with small time steps which will serve as the reference solution. As expected, the streamline solution becomes unstable for $CFL > 1.$ This is consistent with the observations by Osako *et al.* But, how about compressible flow? **Fig. 3.10a** shows the results for a pressure update time step of 20 days. We obtain very good agreement with the finite difference solution for this case. However, as the time step size is increased to 40, and 60 days, the results deviate from the finite difference solution and also show oscillatory behavior, **Fig. 3.10b**. These results are summarized in **TABLE 3.6** which shows that the stable time step is given by *CFL* limit of unity. The unstable time steps are marked yellow.

TABLE 3.5—FLUID PROPERTIES OF WATER AND OIL

	Compressibility [1/psi]	Viscosity [cp]
Water	1.00E-06	1.0
Oil	4.60E-04	0.5

TABLE 3.6—CORRECTION CFL FOR STABILITY

	Time step (days)		
	20	**40**	**60**
CFL-Incompressible	0.716	0.97	1.385
CFL-Compressible	0.727	1.18	2.683
CFL-Compressible FD	13.696	17.969	19.933

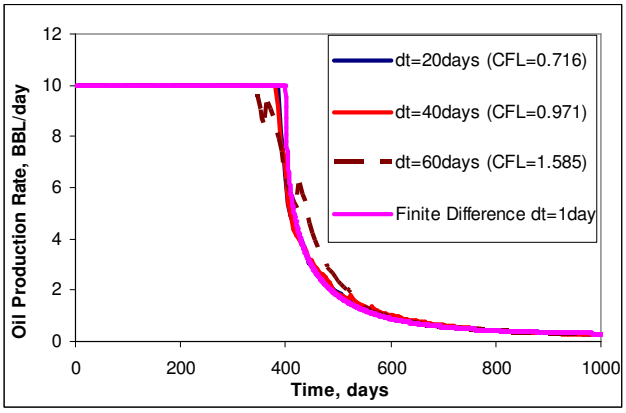

Figure 3.9— Impact of pressure time step size on oil production rate (incompressible flow).

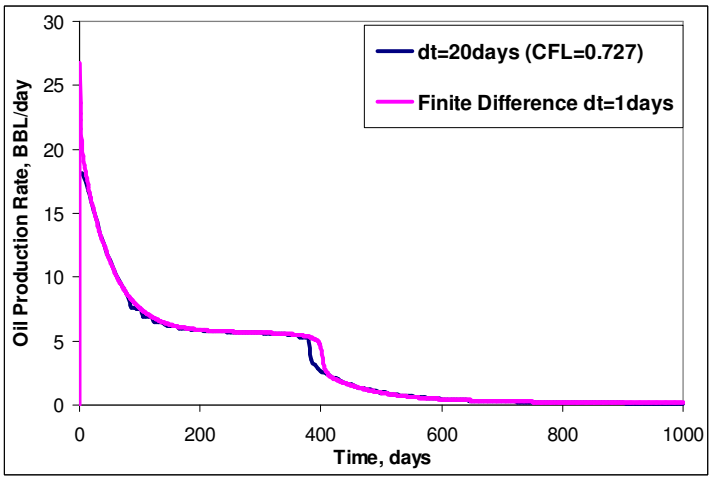

(a) Pressure update time step = 20 days

Figure 3.10— Impact of pressure time step size on oil production rate (compressible flow).

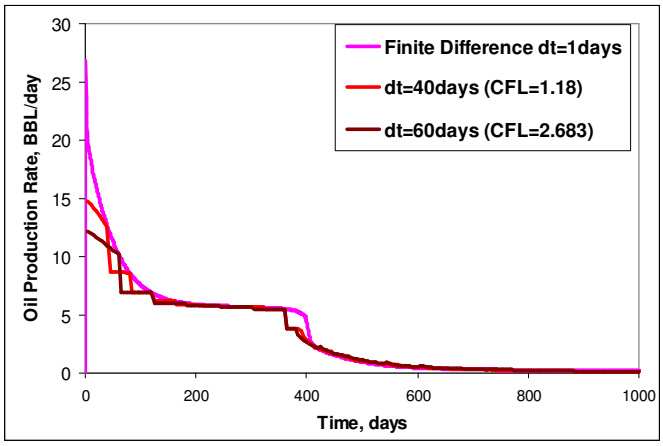

(b) Pressure update time step = 40, 60 days

Figure 3.10— Continued

For comparison purposes, in **TABLE 3.6** we have also shown the CFL numbers computed for the conventional finite difference simulation using the same time steps. Clearly, the finite difference solution is unstable for all the time steps. Based on the results, it appears that the stable time step for finite difference solution for this example will be less than 2 days

3.3 Chapter Summary

We have presented a rigorous formulation for two and three – phase black oil compressible streamline simulation. Unlike previous studies, we no longer assume that volumetric flux is conserved along streamlines. The key features of our formulation are (i) introduction and tracing of an effective density along streamlines to account for fluid expansion/compression, (ii) use of the effective density during mapping from streamlines to grid blocks and vice versa and (iii) a source/sink term in the saturation equation along streamlines to account for compressibility effects. Although we have restricted our development to black oil simulation, the approach is quite general and can be easily extended to compositional simulation. Gravity effects are accounted for using operator splitting as in incompressible streamline simulation [4]. We have validated our approach by comparison with finite difference simulation for two and three phase flow using synthetic and field examples. Importantly, our proposed formulation can be easily implemented within the framework of existing streamline simulators.

Some specific conclusions from this study can be summarized as follows:

1. A rigorous compressible streamline formulation has been presented for two and three-phase black oil simulation. Our proposed approach requires only minor modifications to current streamline simulators with significant improvement in accuracy of performance predictions.
2. We can now account for fluid expansion/compression along streamlines by introducing an effective density along the streamlines. This effective density can be easily traced along the streamline and allows us to rigorously decouple the 3-D saturation equation into a series of 1-D equations.
3. We have reformulated the 1-D saturation equations along streamlines by introducing a source/sink term to account for compressibility effects. Also, the mapping of saturations from streamlines to grid blocks and vice versa has been improved to account for changes in fluid volume.
4. We have shown that the discrete CFL number of Osako *et al.*[14] for selection of time step for pressure updates also applies to compressible streamline simulation. As expected, the compressible formulation restricts the simulation to smaller time-step size compared to incompressible flow in order to maintain the stability of the solution.
5. We have validated our new formulation using synthetic and field examples and comparison with a commercial finite difference simulator.

CHAPTER IV

COMPOSITIONAL STREAMLINE SIMULATION WITH COMPRESSIBILITY EFFECTS

Streamline simulators have been applied in many waterflood projects because of their ability to take large time-steps during the pressure solution in an IMPES formulation under the incompressible fluid flow assumptions. However, the incompressibility assumption limited the application to the reservoirs that do not contain highly compressible fluids such as live oil and gas. Our recently proposed rigorous compressible streamline formulation [2] has overcome the assumptions and we have validated our approach with black oil model examples. The application to compositional simulation is more appealing because of the linear scaling properties in computation time for streamline models.

Our proposed approach for the rigorous compressible formulation is based on three elements. First, we formulate an equation to trace the effective density along the streamline to capture the expansion and shrinkage of the fluid along the streamline. Second, a simple corrector algorithm is used to update the saturation to account for the density changes because of the compressibility. Thirdly, we propose a treatment to reallocate the rate of each streamline based on the density. These three elements will capture all physics of compressibility and also be done all along streamline without going back to grid block domain.

We demonstrated the validity and practical utility of our approach using a series of numerical experiments in a 2-D five-spot pattern, and an application to 3-D heterogeneous case with four components fluid example. For the numerical experiments, we pay particular attention to the importance of rigorous treatment of compressibility which is absent on earlier works.[11-15] Our results clearly demonstrate the impact of the remapping and reallocation algorithms based on the density difference along the streamline because of the compressibility and also the linear scaling advantage of streamline. The proposed approach broadens streamline applications into other types of reservoirs currently not applied in the industry.

4.1 Introduction

In many applications, a black oil representation of the reservoir fluids is inadequate. These include depletion of gas condensate and volatile oil reservoirs and also enhanced oil recovery processes such as enriched miscible gas injection, carbon dioxide flooding and chemical flooding. Specifically, when the fluid properties are dependent on both phase composition and pressure, we have to resort to compositional simulation. Such simulations involve the solution of the mass conservation equation in conjunction with phase equilibrium calculations to determine phase compositions, phase pressures and saturations.[3-5] The additional capabilities of compositional simulation also make it more expensive in terms of computation time and memory. This makes the potential benefit of streamline based compositional simulation even more compelling than for black oil or for two-phase waterflood.

We already know that streamline models can outperform conventional finite difference simulation in terms of computational speed. However, most applications have been limited to incompressible or slightly compressible flow and under convection dominated flow.[8-10, 24-27] The underlying incompressible assumption allows us to decouple the pressure and conservation equations easily by introducing a time of flight coordinate.[1] By applying the time of flight as a spatial coordinate, multidimensional conservation equations are decoupled into series of 1-D equation and the decoupled equation can be solved using a relatively large time step compared to original grid block based equations. The decoupled equation can also reduce numerical dispersion and grid orientation effects which eventually improve the accuracy of the solution.

However, most of the elegance and simplicity of the streamline models are lost once we think about compressible flow because of the coupling between pressure and saturation. Several authors have attempted to overcome the incompressibility assumptions during streamline simulation.[2, 11-15] Since the pressure and velocity calculations in streamline models use finite difference scheme, most of these previous works have rigorously accounted for compressibility effects in the pressure equation. However, all of these formulations neglect the divergence of total flux term during the derivation of 1-D conservation equations. The divergence of total flux term is essential to account for compressibility effects because it vanishes for incompressibility assumptions. Neglecting this term is not only incorrect for compressible flow but also introduces inconsistency between the pressure and conservation equations. All these lead to increased material balance error and very often inaccurate performance predictions.

Our recent proposed approach [1] removed the limitation for two and three- phase black oil simulation by introducing relative density concepts and mapping the relative density along streamline. The divergence of total flux representing the fluid expansion/compression is captured by the relative density. The conservation equations are decoupled into series of 1-D equation and the divergence of total flux acts as a source term. Following are the basic objectives in this study:

- Introduce the compressible streamline formulation and highlight the main differences with the existing incompressible formulation.
- Present several examples to outline the major steps and illustrate the underlying concepts in compressible streamline simulation.
- Derive the 1-D conservation equations along streamlines for compositional model.
- Apply our 1-D conservation equations into UTCOMP
- Validate the new formulation by comparison with finite difference simulation

In this study, we apply a finite difference simulator (UTCOMP) [6] for pressure and streamline trajectory. Our new approach is used in conservation equation part in evolving phase compositions and saturations.

For our validation purpose, our streamline model is compared with the finite difference compositional simulation results obtained from UTCOMP.

4.2 Compositional Streamline Formulation

Much of the elegance of the current streamline (or streamtube) formulation arises from the restriction to incompressible flow. In short, if a specific volumetric flux is allocated to a line or a tube at an injector, then that same flux will be transported to a producer. However, most real systems have some degree of compressibility. The compressibility effects become particularly important for three-phase flow including gas. Thus, the formulation needs to be generalized to account for changes in fluid volumes because of pressure variations along the streamwise directions. Fortunately, a small modification to the equations presented so far can be used to determine the volumetric flux as a function of distance along a streamline. A similar approach could be applied to streamtube calculations, although historically this has not been implemented.

Fig. 4.1 shows the flowchart of compositional streamline simulation. After initializing reservoir and well parameters, we can obtain pressure and corresponding velocity fields on simulation grid blocks. Streamline tracing starts from producers to injectors with the velocity fields and we sample several parameters required for phase flash calculations and solution of conservation equations along streamlines. We evolve compositions along the streamline with a series of 1D conservation equations. Evolved parameters will be sampled back to grid blocks and updated by operator splitting technique [10, 28, 29] if gravity effects are dominant. We continue the loop until the end of simulation time.

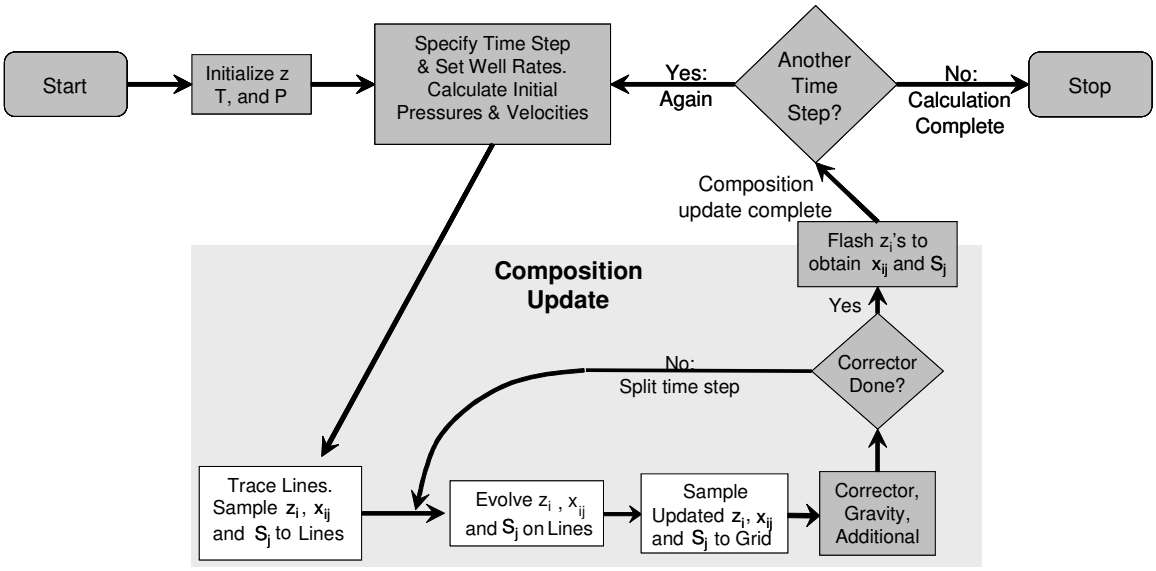

Figure 4.1— Flow chart of compositional streamline simulation.

4.2.1 Pressure Calculation of Compositional Streamline Simulation

Streamline simulation is an IMPES type reservoir simulation, which solves pressure equation implicitly followed by saturation equation or conservation equation explicitly. Streamline simulation starts by solving pressure equation. Here we discuss how we solve pressure equation in compositional simulation. Since the essence of streamline simulation is coordinate transformation from 3-D physical space to 1-D time of flight along streamline, there is no special treatment for solution of pressure equation compared to conventional finite difference approach. Let us start by clarifying the difference of pressure equation between the black oil and compositional case. In the black oil case, we are able to eliminate the derivative

term of saturation with respect to time so that we could obtain the pressure equation easily. However, in compositional case we can not eliminate the term directly to get the pressure equation. Thus, we need iterative solutions to handle the non-linearity of accumulation terms. In this study, we apply the technique introduced by Acs *et. al.* [30] and Watts.[31] They have introduced a 'volume balance' formulation, which tries to balance the pore volume of the reservoir and the total fluid volume. The balanced system is simply the pore volume filled totally with the fluids. Our derivation came directly from an overall system volume balance in stead of working with individual phase equations. In the balanced system, we have

$$V_t(P,N) = V_p(P) \text{ .....} \tag{4.1}$$

where the total fluid volume, V_t, is a function of pressure and fluid composition, and the rock pore volume, V_p is a function of only the pressure. Here, N denotes the fluid composition given by the total number of moles of each component, N_i, $i = 1,2,\ldots,n_c$. Differentiating **Eq. 4.1** with respect to time and using the chain rule, we obtain

$$\left(\frac{\partial V_t}{\partial P}\right)_N \left(\frac{\partial P}{\partial t}\right) + \sum_{i=1}^{n_c} \left(\frac{\partial V_t}{\partial N_i}\right)_{P,N_k(k\neq i)} \left(\frac{\partial N_i}{\partial t}\right) = \left(\frac{\partial V_p}{\partial P}\right)\left(\frac{\partial P}{\partial t}\right) \tag{4.2}$$

Let us define ϕ^0 and V_p^0 to be the porosity and pore volume at a reference pressure P^0. From the definition of rock or formation compressibility c_f we have the following,

$$\phi = \phi^0[1 + c_f(P - P^0)] \text{ .....} \tag{4.3a}$$

$$\left(\frac{\partial V_p}{\partial P}\right) = V_p{}^0 c_f \text{ .....} \tag{4.3b}$$

The general mass conservation equation is given by,

$$\frac{\partial W_i}{\partial t} + \nabla \bullet \left(\sum_{j=1}^{n_p} \xi_j S_j \vec{u}_j - \phi \xi_j S_j \vec{\vec{K}} \bullet \nabla x_{ij} \right) - q_i = 0 \cdots \tag{4.4}$$

Where, W_i in **Eq. 4.4** represents the number of moles of component i per unit bulk volume. Thus, the total number of moles of component i, N_i will be given by,

$$N_i = V_b W_i = V_b \phi \sum_{j=1}^{n_p} \xi_j S_j x_{ij} \quad \text{.....} \tag{4.5}$$

Here, V_b is the bulk volume. The mass conservation equation, **Eq. 4.4** can now be expressed as follows,

$$\frac{\partial N_i}{\partial t} + V_b \nabla \bullet (\sum_{j=1}^{n_p} \xi_j x_{ij} \vec{u}_j - \phi \xi_j S_j \vec{\vec{K}} \bullet \nabla x_{ij}) - q_i V_b = 0 \tag{4.6}$$

Here, $\vec{\vec{K}}$ is the dispersion tensor, not to be confused with the permeability tensor, $\vec{\vec{k}}$. At this stage, it is convenient to introduce the concept of the partial molar volume defined by,

$$\overline{V}_{ti} = \left(\frac{\partial V_t}{\partial N_i} \right)_{P, N_k (k \neq i)} \qquad i = 1, \ldots, n_c \quad \text{.....} \tag{4.7}$$

The partial molar volume represents the change in total volume as a mole of component *i* enters or leaves the system. It can be computed directly from the equation of state or from empirical fluid property correlations.

Substituting **Eq. 4.3b**, **Eq. 4.6** and **Eq. 4.7** into **Eq. 4.2**, we obtain a preliminary form of the compositional pressure equation,[32]

$$\left(\frac{\partial V_t}{\partial P} \right) \left(\frac{\partial P}{\partial t} \right) - V_b \sum_{i=1}^{n_c} \overline{V}_{ti} \nabla \bullet \left(\sum_{j=1}^{n_p} \xi_j x_{ij} \vec{u}_j - \phi \xi_j S_j \vec{\vec{K}} \bullet \nabla x_{ij} \right) + V_b \sum_{i=1}^{n_c} \overline{V}_{ti} q_i = V_p{}^0 c_f \left(\frac{\partial P}{\partial t} \right) \tag{4.8}$$

The phase velocities $\vec{u}_j$ can be expressed in terms of phase pressures using Darcy's law. We can utilize the capillary pressure relationships to replace all other phase pressures in terms of a reference phase pressure, for example phase 1, $P = P_1$. Suppose, $P_{c\ell j} = P_j - P_\ell$, for example, $P_j = P_1 + P_{c1j}$, and $P_{c11} = 0$.

$$\left(V_p^0 c_f - \frac{\partial V_t}{\partial P}\right)\left(\frac{\partial P}{\partial t}\right) = V_b \sum_{i=1}^{n_c} \overline{V}_{ti} q_i + V_b \sum_{i=1}^{n_c} \overline{V}_{ti} \nabla \bullet \left(\sum_{j=1}^{n_p} \left(\lambda_{rj} \xi_j x_{ij} \vec{\vec{k}} \bullet \left(\nabla P + \nabla P_{c1\,j} - \rho_j g \nabla D \right) + \phi \xi_j S_j \vec{\vec{K}} \bullet \nabla x_{ij} \right) \right) \quad \text{.....} \tag{4.9}$$

Again, the pressure equation **Eq. 4.9** is solved using finite difference methods. The solution of the pressure equation requires the evaluation of the partial derivatives of total volume with respect to pressure and component moles. These derivatives can be calculated from the equation of state and the phase equilibrium relations.

4.2.2 Extension of Rigorous Compressible Formulation to Compositional Model

Once we solve for pressure and obtain the velocity field on grid blocks, we can trace streamlines and map underlying grid properties onto the streamlines. Along each streamline, we will evolve compositions with the conservation equation. In this section, we will show how to decouple the 3-D conservation equation into a series of 1-D equations by applying rigorous compressible streamline formulation.[2] The general conservation equations for multi-component multiphase flow in the absence of sources or sinks is given by **Eq. 4.10**. For clarity of exposition, we will neglect physical dispersion,

$$\frac{\partial}{\partial t}\left(\phi \sum_{j=1}^{n_p} \xi_j S_j x_{ij} \right) + \nabla \bullet \left(\sum_{j=1}^{n_p} \xi_j x_{ij} \vec{u}_j \right) = 0 \text{ .....} \tag{4.10}$$

The phase velocities can be expressed in terms of total velocity using Darcy's law as in **Eq. 4.11**,

$$\vec{u}_j = F_j \vec{u} + \sum_{\ell=1}^{n_p} \frac{\lambda_{rj} \lambda_{r\ell}}{\lambda_{rt}} \vec{\vec{k}} \bullet \left(\nabla P_{cj\ell} + \Delta \rho_{\ell j} g \nabla D \right) \text{ .....} \tag{4.11}$$

Here, $P_{cj\ell} = P_\ell - P_j$, $\Delta \rho_{\ell j} = \rho_\ell - \rho_j$, and $F_j = \dfrac{\lambda_{rj}}{\lambda_{rt}}$.

During streamline simulation the gravity and capillary pressure terms are treated using operator splitting as discussed before. We will focus on the convective flux term to derive the compositional streamline equation. Expanding the divergence operator in **Eq. 4.10**, we get

$$\nabla \bullet \left(\sum_{j=1}^{n_p} \xi_j x_{ij} F_j \vec{u} \right) = \vec{u} \bullet \nabla \left(\sum_{j=1}^{n_p} \xi_j x_{ij} F_j \right) + (\nabla \bullet \vec{u}) \left(\sum_{j=1}^{n_p} \xi_j x_{ij} F_j \right) \tag{4.12}$$

The usual definition of the time of flight, τ, and the definition of c for compressible systems provide us with:

$$\vec{u} \bullet \nabla = \phi \frac{\partial}{\partial \tau} \quad and \quad \nabla \bullet \vec{u} = c$$

This leads to the following component conservation equation along streamlines,

$$\frac{\partial z_i}{\partial t} + \frac{\partial j_i}{\partial \tau} = -\frac{c}{\phi} j_i \text{ .....} \tag{4.13}$$

Here, z_i is the total mole number per unit pore volume for component i and is given by,

$$z_i = \sum_{j=1}^{n_p} \xi_j S_j x_{ij} \text{ .....} \tag{4.14}$$

In deriving **Eq. 4.13**, we have neglected porosity changes with time for simplicity. This can be easily avoided by including porosity in the definition of z_i. The fractional flux of component i has been defined by

$$j_i = \sum_{j=1}^{n_p} \xi_j x_{ij} F_j \text{ .....} \tag{4.15}$$

so that the flux of component i is given by

$$\vec{J}_i = j_i \vec{u} \text{ .....} \tag{4.16}$$

Same as black oil example, the source / sink term $\left(-\frac{c}{\phi} j_i \right)$ in **Eq. 4.13** is very important to correctly model flow along the streamlines. Early treatments of compositional streamline

simulation [11, 14, 15] were developed in the incompressible limit ($c \to 0$) and did not include this term.

Eq. 4.13 can be solved numerically for z_i along each streamline. The total composition is mapped back onto the grid at the end of the pressure time step. Note that during mapping, we must account for fluid expansion using the 'effective density' term in compressible flow as discussed well in our previous chapter. Thus, the total composition in a streamline segment within a grid block should be weighted by $d\tau/\rho$ for that streamline segment while mapping onto the grid. The gravity and capillary pressure terms can be accounted for at this stage via operator splitting. Finally, the phase compositions and saturations are obtained from the total composition by thermodynamic flash calculations.

4.2.3 Phase Equilibrium Calculation

Reviewing **Fig. 4.1**, almost all aspects of compositional streamline simulation have been discussed except the phase equilibrium calculations. The solution of the 1-D conservation equations, **Eq. 4.13** yields updated z_i, the overall composition along the streamlines. Phase equilibrium or 'flash' calculations are required to determine the number of hydrocarbon phases, the phase saturations, S_j and their compositions, x_{ij}, at a given temperature and pressure. Compositional simulation involves frequent flash calculations and thus, it is necessary that these calculations be efficient and robust. In general, phase equilibrium calculations impose three conditions. First, the overall material balance (molar balance constraints) must be satisfied for each component. Second, the chemical potential (or equivalently, the fugacities) of each component must be the same in all phases. Finally, the equilibrium phase split and composition must have the lowest Gibbs free energy at the given temperature and pressure.[33]

The details of the phase equilibrium calculations are the same as for finite difference simulation. The calculations typically follow a sequential application of phase stability analysis to determine the number of phases followed by flash calculations to determine the amount and composition of each phase.[32, 34, 35] The phase stability analysis ensures that the Gibbs free energy is minimized for the number of phases in equilibrium. The flash calculations involve an iterative procedure to compute the equilibrium constants or K-values defined as the ratio of the component mole fractions in the vapor and the liquid phases. The basis for computing the K-

values is the equality of the component fugacities in each phase. The component fugacities can be conveniently obtained using an equation of state such as the Peng-Robinson equation of state.[36]

4.2.4 Solution of the Conservation Equation

The 1-D compositional transport equation has been reduced to the simple form, **Eq. 4.13.** As in the case of waterflooding, the transport equations can be solved analytically for two-phase multi-component incompressible flow with constant initial and injection conditions.[37-38] The analytic solutions are constructed by solving the eigenvalue problems associated with the mass conservation equations and involve Riemann solutions. The goal here is to identify the unique path (composition route) that connects the initial and injection conditions in the composition space.[39, 40] When applicable, these analytic solutions can lead to significant savings in computation time. However, for most practical situations, a numerical solution will be necessary. The transport equation along a streamline, **Eq. 4.13**, can be approximated by finite difference as follows,

$$\frac{(z_i)_\ell^{n+1} - (z_i)_\ell^n}{\Delta t} + \frac{(\bar{j}_i)_{\ell+1/2} - (\bar{j}_i)_{\ell-1/2}}{\Delta \tau} = -\frac{c}{\phi} j_i \quad i = 1,\ldots,n_c \tag{4.17}$$

where ℓ is the spatial discretization index in the τ direction, and $(\bar{j}_i)_{\ell+1/2}$, $(\bar{j}_i)_{\ell-1/2}$ represent the time-averaged flux of component i at the node boundaries and are given by,

$$(\bar{j}_i)_{\ell+1/2} = \left(\sum_{j=1}^{n_p} \xi_j x_{ij} F_j \right)_{\ell+1/2}^{n+1/2} \quad \text{.....} \tag{4.18a}$$

$$(\bar{j}_i)_{\ell-1/2} = \left(\sum_{j=1}^{n_p} \xi_j x_{ij} F_j \right)_{\ell-1/2}^{n+1/2} \quad \text{.....} \tag{4.18b}$$

The simplest approximation to the fluxes at the node boundaries is the single-point upstream weighting which yields smooth and stable solutions. This leads to the following finite difference form,

$$\frac{(z_i)_\ell^{n+1}-(z_i)_\ell^n}{\Delta t}+\frac{(j_i)_\ell^n-(j_i)_{\ell-1}^n}{\Delta\tau}=-\frac{c}{\phi}j_i \quad \text{.....} \tag{4.19}$$

Here expressed for flow in the direction of increasing ℓ, or equivalently with increasing τ.

4.2.5 Validation of the Method

We now validate the calculations using CO2 injection into a depleted oil and gas reservoir in a homogeneous five-spot pattern using 4 components and compare the results with the finite-difference compositional simulation. The initial reservoir pressure was set at 1200 psi and the four corner producers are bottomhole pressure constrained at 1000 psi. Properties for each component are summarized in **TABLE 4.1**. The velocity field obtained from the pressure distribution is used to trace streamlines and compute time of flight using the Pollock algorithm [17] as in the conventional streamline case. Note that the Pollock algorithm is sufficiently general and is not limited to incompressible flow. However, unlike incompressible flow, streamlines can now originate and terminate anywhere in the domain.

TABLE 4.1—FLUID PROPERTIES OF COMPONENTS

Component	Critical Pressure	Critical Temperature	Critical Volume	Molecular Weight
	[psi]	[R]	[ft3/lb-mole]	[lb/lb-mole]
CO2	1070.6	547.43	1.507	44.01
C1	667.1961	343.08	1.5798	16.043
C4-6	485.939	839.538	5.0201	72.824
C7-14	351.535	1085.53	8.8842	135.8191
	Acentric Factor	Parachor	Volume Shift Parameter	
CO2	0.22394	78	0.14	
C1	0.01142	71	-0.154	
C4-6	0.2436	233.048	0.0406	
C7-14	0.6	394.499	0.0634	

The cumulative oil rate at the producing wells for the compositional streamline calculations is shown in **Fig. 4.2**. For validation purposes, we have also shown the results from finite difference simulation. There is very good agreement between streamline and finite difference calculations. To demonstrate the effects of fluid compressibility, we have also superimposed the results without the compressibility term on **Eq. 4.13** which captures the fluid expansion/compression. Clearly, the compressibility effects are too large to be ignored for this case. **Fig. 4.3** shows the

cumulative gas comparisons in this case. Again we have very good agreement between streamline and finite difference calculation.

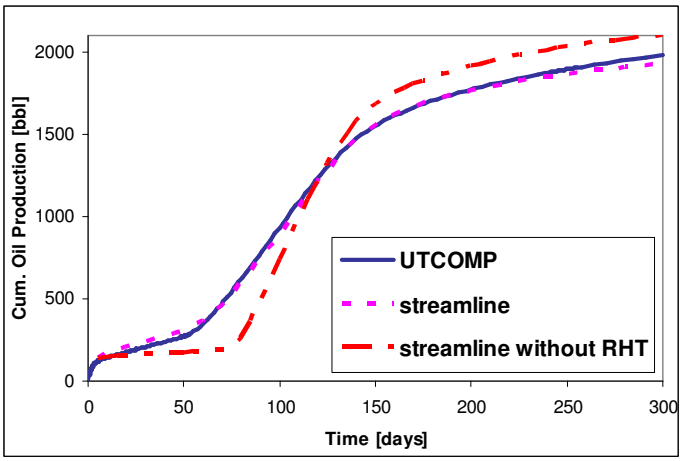

Figure 4.2— Cumulative oil production rate comparisons including without RHT.

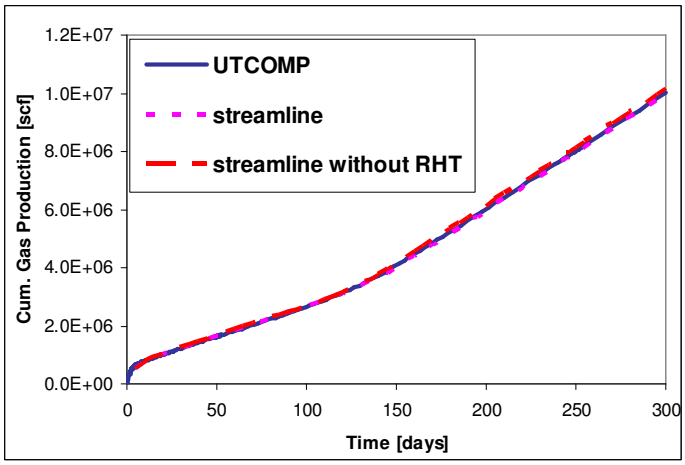

Figure 4.3— Cumulative gas production rate comparisons including without RHT.

4.2.6 High Resolution Numerical Scheme

Because of the rapid mobility and composition changes in compositional simulation, the single point upstream weighting in **Eq. 4.19** can produce unacceptably smeared results when applied to problems that entail propagating sharp or unstable fronts. Numerical dispersion can be particularly pronounced in compositional simulation because unlike waterflooding, the saturation

or composition front may not be self-sharpening. Also, numerical dispersion can interact with phase behavior leading to phase trapping and inaccurate recovery predictions.[41] To remedy the situation, the industry has focused on high resolution numerical schemes for compositional simulation. By such schemes, we imply numerical methods that are at least second-order accurate in the smooth regions and yet give well resolved, non-oscillatory fronts.[42]

In this section we will develop a widely used class of high resolution numerical schemes known as Total Variation Diminishing (TVD) schemes.[43] The TVD schemes utilize flux limiters to selectively restrict higher order fluxes to prevent non-physical oscillations. In practice the TVD schemes will be applied to each component flux in the form

$$\left(\bar{j}_i\right)_{\ell+1/2} = \left(j_i\right)_\ell^n + \varphi(r)\frac{\left(j_i\right)_{\ell+1}^n - \left(j_i\right)_\ell^n}{2}\left(1-\frac{\Delta t}{\Delta \tau}\right) \ldots \tag{4.20}$$

where

$$r = \frac{\left(j_i\right)_\ell^n - \left(j_i\right)_{\ell-1}^n}{\left(j_i\right)_{\ell+1}^n - \left(j_i\right)_\ell^n} \ldots\ldots\ldots\ldots\ldots\ldots\ldots\ldots\ldots\ldots\ldots\ldots \tag{4.21}$$

The flux limiting function $\varphi(r)$ in Leonard Scheme (third order) [44] will be defined as

$$\varphi^{LE}(r) = \frac{2-\lambda}{3} + \frac{1+\lambda}{3}r \ldots\ldots\ldots\ldots\ldots\ldots\ldots\ldots\ldots\ldots\ldots\ldots \tag{4.22}$$

We know that the direct application of higher order schemes can result in oscillatory solutions for the propagation of sharp fronts. Sweby [45] derived the algebraic conditions on the limiter function $\varphi(r)$ that guarantees monotonicity and prevents non-physical oscillations in the solution.

$$0 \le \frac{\varphi(r)}{r}, \varphi(r) \le 2 \ldots\ldots\ldots\ldots\ldots\ldots\ldots\ldots\ldots\ldots\ldots\ldots \tag{4.23}$$

Recall that our goal is to derive difference schemes that minimize numerical diffusion, whilst maintaining monotonicity. Thus, we want to maximize the contribution of the higher-order anti-diffusive flux in **Eq. 4.20**, without violating the conditions of **Eq. 4.23**. To limit each of the flux functions, at each value of r, we have applied the criteria below for Third-order Leonard,

$$\varphi^{LE}(r) = Max\left[0, Min\left(2, 2r, \phi^{LE}(r)\right)\right] \ldots\ldots\ldots\ldots\ldots\ldots \quad (4.24)$$

Figs. 4.4 and 4.5 show comparisons of cumulative oil & gas production results from finite difference and our streamline simulation both with TVD scheme. Overall, we obtained the reasonable agreement. And also if we compare to **Figs. 4.2 and 4.3** obtained with single point upstream weighting, oil and gas production seem accelerated a bit with high order numerical schemes. It means the numerical dispersion because of single point upstream is reduced by introducing the high order numerical scheme.

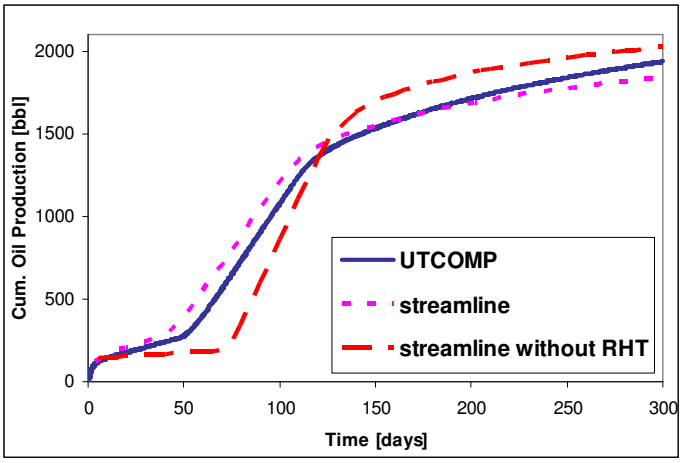

Figure 4.4— Cumulative oil production rate comparisons with TVD including without RHT.

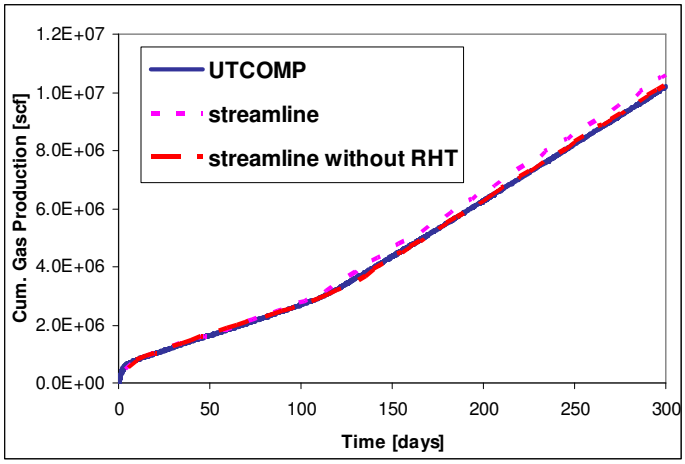

Figure 4.5— Cumulative gas production rate comparisons with TVD without RHT.

4.2.7 Gravity Segregation in Compositional Streamline Simulation

As in the black oil case, the operator splitting method has been applied to capture gravity segregation in compositional streamline simulation. Jessen *et al.* [28] has already presented the details of the technique based on the operator splitting as applied in the black oil case. By substituting **Eq. 4.11** into **Eq. 4.10**, the conservation equation will be given by,

$$\frac{\partial}{\partial t}\left(\phi\sum_{j=1}^{n_p}\xi_j S_j x_{ij}\right)+\nabla\bullet\left\{\sum_{j=1}^{n_p}\xi_j x_{ij}F_j\vec{u}+\sum_{j=1}^{n_p}\xi_j x_{ij}\left[\sum_{l=1}^{n_p}\frac{\lambda_{rj}\lambda_{rl}}{\lambda_{rt}}\vec{\vec{k}}\left(\nabla P_{cjl}+\Delta\rho_{lj}g\nabla D\right)\right]\right\}=0 \tag{4.25}$$

We neglect the capillary pressure and now apply operator splitting technique. Then, we obtain the following two equations,

$$\frac{\partial}{\partial t}\left(\phi\sum_{j=1}^{n_p}\xi_j S_j x_{ij}\right)+\nabla\bullet\left(\sum_{j=1}^{n_p}\xi_j x_{ij}F_j\vec{u}\right)=0 \cdots\cdots\cdots\cdots \tag{4.26a}$$

$$\frac{\partial}{\partial t}\left(\phi\sum_{j=1}^{n_p}\xi_j S_j x_{ij}\right)+\frac{\partial}{\partial z}\left(\sum_{j=1}^{n_p}\xi_j x_{ij}\sum_{l=1}^{n_p}\frac{\lambda_{rj}\lambda_{rl}}{\lambda_{rt}}k_z\Delta\rho_{lj}g\right)=0 \tag{4.26b}$$

Eq. 4.26a eventually leads to the same form as **Eq. 4.13** and is solved along streamlines. **Eq. 4.26b** is solved on each grid block with the following equation,

$$\frac{\partial z_i}{\partial t}+\frac{1}{\phi}\frac{\partial}{\partial z}\left(\sum_{j=1}^{n_p}\xi_j x_{ij}\sum_{l=1}^{n_p}\frac{\lambda_{rj}\lambda_{rl}}{\lambda_{rt}}k_z\Delta\rho_{lj}g\right)=0 \quad \text{.....} \tag{4.27}$$

Jessen *et al.* [28] introduced a pseudo-immiscible approach to reduce the CPU time as well as the operator splitting error. Their proposed method updates saturations instead of component moles along gravity lines at the end of convective step. When we map parameters back to grid block from streamlines, all parameters such as phase saturation, densities, and viscosities are already known. Then we can update phase saturations by using the modified version of the approach for black oil model (**Eq. 3.18** in the last chapter).

$$S_{i,k}^{n+1}=S_{i,k}\Big|^n-\frac{\Delta t}{\phi\Delta z}\left(G(S)\Big|_{i,k+1/2}^n-G(S)\Big|_{i,k-1/2}^n\right)\text{.....} \tag{4.28}$$

where, *i* is either liquid or gas.

Once we update phase saturations based on the gravity force, we need to update overall mole fraction and molar density for new time step pressure calculations.

4.2.8 A 3-D Heterogeneous 5 Spot Example

We simulated again CO2 injection for a depleted reservoir in a five-spot pattern. A heterogeneous permeability model with 21×21×4 grid cells was used, and the permeability field is shown in **Fig. 4.6.** It was generated by sequential Gaussian simulation. Since it is a three dimensional model, we have applied the gravity segregation treatment for our compositional model.

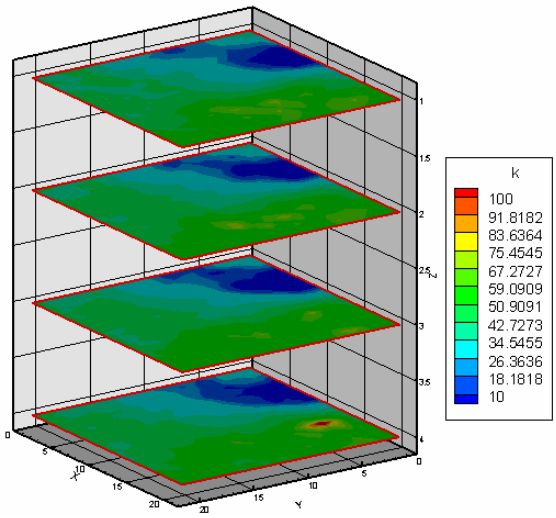

Figure 4.6— Heterogeneous permeability field.

Jessen and Orr [28] proposed a pseudo-immiscible approach for the treatment of gravity segregation with compositional streamline model. It involves solving the gravity lines just after the end of a given convective step as in conventional operator splitting approaches. The initial water saturation is 0.25. Initial reservoir pressure is 1200 psi, and we have four different initial components (CO2=0.05, C1 = 0.35, C4-6 = 0.45, C7-14 = 0.15) and their properties are same as in the last 2-D example. The producer is bottomhole pressure constrained at 1000 psi, and the injector is rate constrained at 500 lbm-mol/day. **Figs. 4.7** show the cumulative oil and gas production rate. Our results show good agreement with the finite difference simulator.

Spatial distribution of gas saturation is also compared in **Figs. 4.8**, where the left side shows results from the finite difference simulator and the right one is from our streamline simulation. It shows a reasonable match except for the bottom layer. We think it is partly because of the difference in injection well treatments between finite difference and streamline simulation. Our streamline simulator is designed to give always 100 % of injection fluid or gas into the injection grid; however, the finite difference simulator will simply solve the material balance in the injection wells. Thus, although the last layer in the finite difference model couldn't inject much volumes compared to the upper layers because of throughput constraints at the injection well, the streamline simulator is able to inject high percentages of gas into the last layer. **Fig. 4.9** shows the spatial distribution of gas saturation without the gravity segregation option in streamline simulation. We can not observe any gas override to the top of the reservoir.

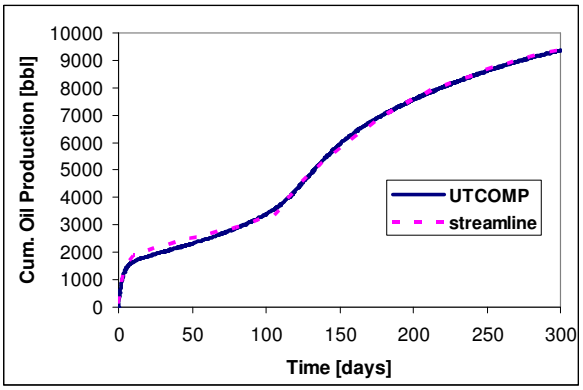

(a) Oil

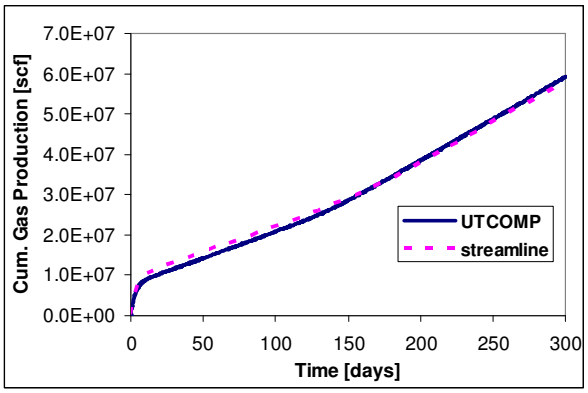

(a) Gas

Figure 4.7— Cumulative well production comparison.

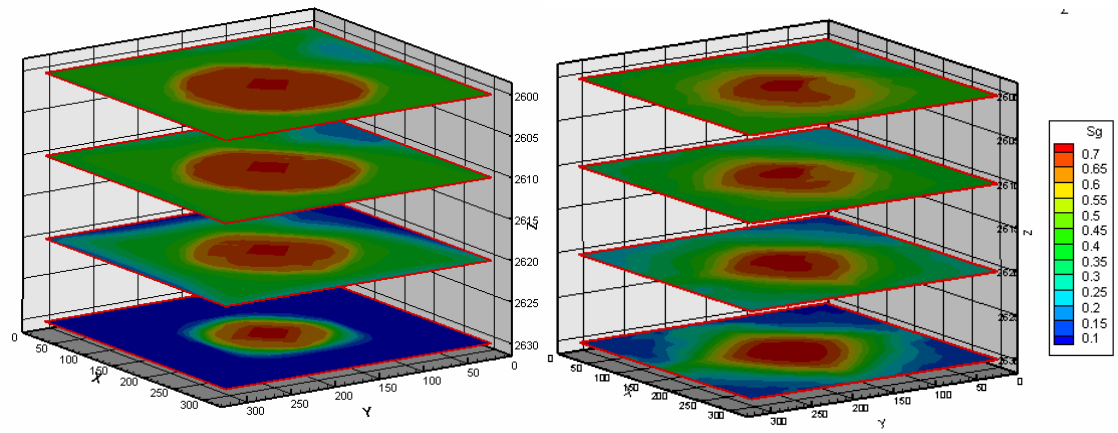

(a) UTCOMP (b) streamline

Figure 4.8— Spatial distribution of gas saturation.

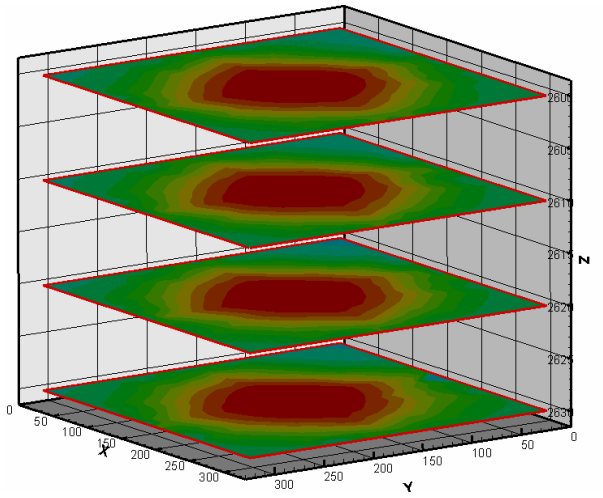

Figure 4.9— Spatial distribution of gas saturation without gravity option in streamline.

As for the CPU time, finite difference simulation took 24 mins, whereas the streamline model took 20 mins.

4.3 Chapter Summary

In this chapter, our rigorous compressible streamline formulation is extended to compositional model. It is quite easy to couple our formulation into existing finite difference simulation. Through the extension, we have demonstrated the importance of higher order numerical schemes and gravity segregation problems for compositional simulation. By including higher order numerical schemes and operator splitting techniques, the streamline simulation is more accurate and physically representative.

Some specific conclusions from this study can be summarized as follows:

1. Use of the relative density term allows us to include compressibility effects in compositional streamline simulation. It retains a source term in compositional streamline equation that can rigorously account for compressibility effects.
2. The relative density traced along streamline decouples 3-D compositional equations to a series of 1-D equations. We can retain the advantage of streamline simulation by taking larger time step size for the 1-D solution along streamlines.

3. We have presented numerical examples to illustrate the importance of including compressibility effects in compositional streamline simulation.

We will discuss the computational time comparison with finite difference simulation in the next chapter.

CHAPTER V

OPTIMAL COARSENING OF STREAMLINE SEGMENTS FOR TRANSPORT CALCULATIONS

As we mentioned in the last section, the numerical dispersion in compositional simulation would be one of the issues we need to pay attention. To reduce the numerical dispersion, one way is to introduce higher order numerical schemes shown in the last section, and another way is to apply finer scale cells for the composition propagation. In streamline simulation, a series of 1D composition propagations are carried out along streamlines and we map the updated compositions onto the grid block. Thus, instead of refining grid blocks in the reservoir model we can refine the segments in each streamline to reduce numerical dispersion. However, the refining of grid blocks or segments along streamlines will lead to increase computation time because we need flash calculations on these blocks or segments, and the flash calculation constitutes much of the computational expenses. In this chapter, we propose a novel approach that optimizes the number of segments along streamline to reduce the computational time during compositional streamline simulation significantly. Let us start by showing the impact of different number of discretization segments along streamline.

5.1 Introduction

Although using streamline simulator we could obtain a reasonable match with finite difference simulation for well performance such as cumulative productions of oil and gas, comparisons of saturation contour profiles show differences especially around injection wells as shown in **Fig. 5.1**. We couldn't improve the results even after introducing higher order numerical schemes. We found that the parameter that determines the number of discretization segments along streamline has a significant impact on the saturation profile. In streamline simulation, once we trace the streamlines, we map grid block parameters onto the streamlines and transform 3-D transport equations from physical space to 1-D time of flight space. **Fig. 5.2a** shows the illustration of a traced streamline. The properties on underlying grid blocks are mapped onto the 1D time of flight coordinate domain as shown in **Fig. 5.2b**, where the left boundary is the

injection well and the right boundary is the producing well. Generally the properties are mapped to irregular time of flight segments. In our calculation, we divide the irregular time of flight segments into regular time of flight segments as shown in **Fig. 5.2c** so that $\Delta\tau$ of the discretized conservation equation (**Eq. 4.17**) would be constant all along the streamline. When we divide into finer segments, we use a parameter to determine the multiplication factor to refine the segments. Suppose one streamline is passing through 20 grid blocks. The refinement parameter is multiplied by the number of grid block to determine the level of discretization. The segments are evenly spaced according to time of flight along the streamline. In **Fig. 5.1,** the refinement factor is 2. **Fig. 5.3** uses a refinement factor of 4, and clearly shows improvement in results. However, the disadvantage of increasing the number of segments along streamlines is to increase the computational time from 8 mins to 32 mins. Now the question is do we really need to refine the segments all along the streamline evenly or can we optimize the level of discretization.

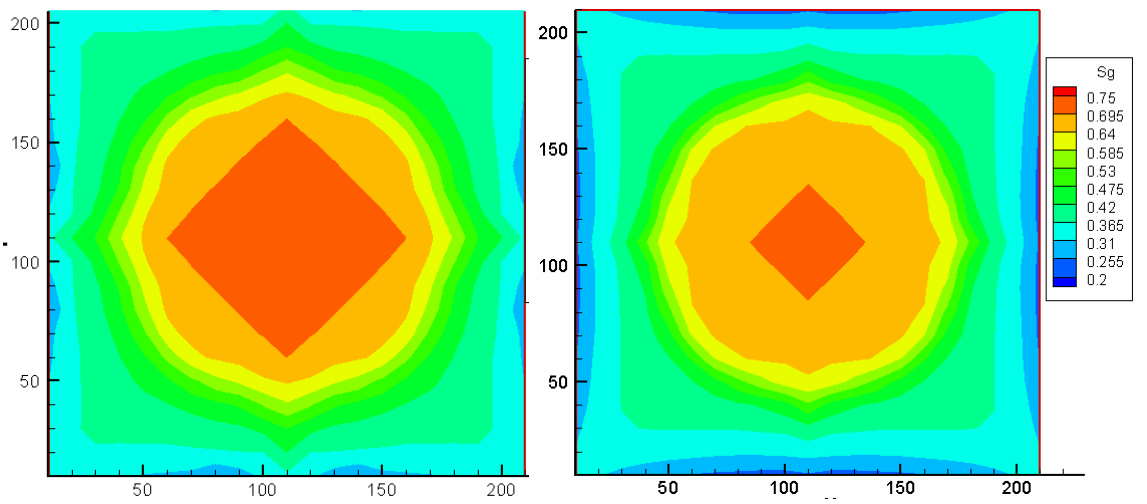

(a) Streamline (factor of refinement = 2) (b) Finite difference

Figure 5.1— Spatial distribution of gas saturation.

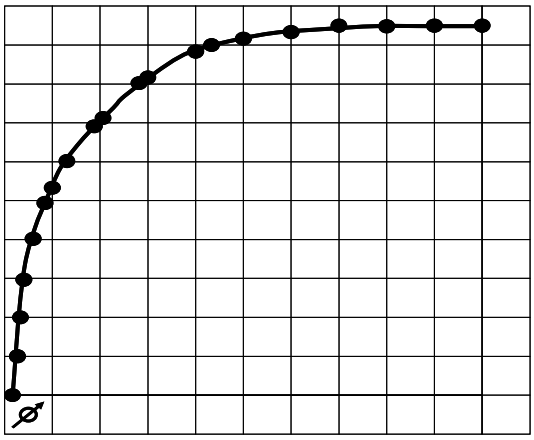

(a) Segments on the traced streamline

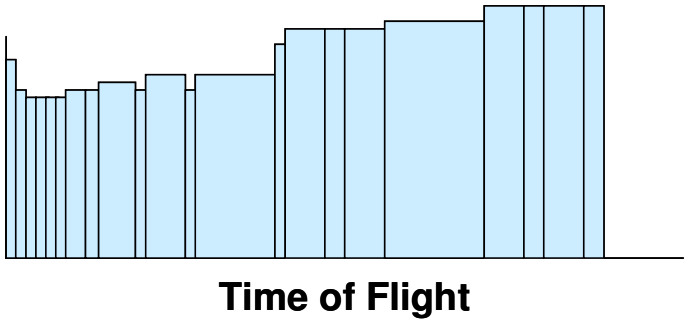

(b) Illustration of segments on irregular time of flight coordinate along streamline

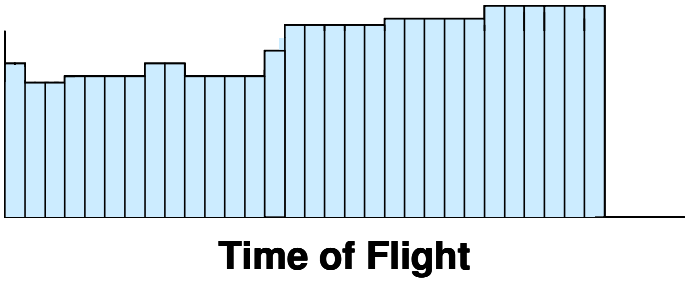

(c) Illustration of segments on regular time of flight coordinate along streamline

Figure 5.2— Illustration of segments along streamline.

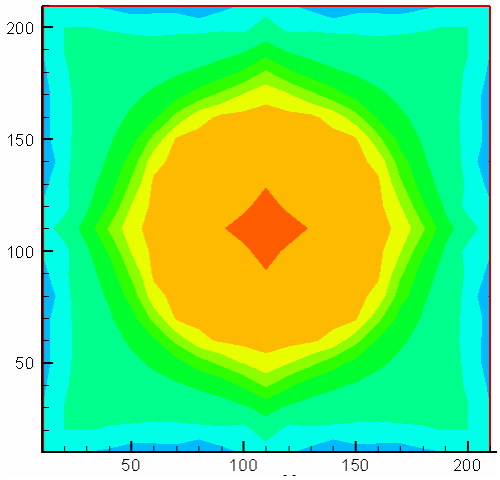

Figure 5.3— Spatial distribution of gas saturation.

5.2 Approach

5.2.1 Optimal Coarsening of Streamline Segments

We have seen the impact of the level of discretization of segments along streamline. How can we define the optimal number of segments? We can think of two ways to define the optimal segments along streamlines. First, one approach would be introducing the adaptive mesh refinement algorithm widely applied in the reservoir simulation.[46] Another approach would be analogous to recursive sequential coarsening applied in the area of upgridding of geological properties.[7, 8, 47, 48] In our study, we examined the optimal coarsening idea given by Testerman,[7] and King *et al.*,[8] because recursive coarsening is significantly faster than the sequential refinement. Also it requires minor modification to our existing code. The original motivation of King *et al.* was to investigate how many layers are required to preserve fine-scale vertical heterogeneity. Their method is quite simple. They introduces sum of squares criteria given by two equations below,

- Sum of squares within layer

$$SSW = \sum_{i=1}^{N_x} \sum_{k=1}^{N_z} \left(p_{ik}^{f} - p_{ik}^{c} \right)^2 \quad \text{.....} \tag{5.1}$$

- Sum of squares between layers

$$SSB = \sum_{i=1}^{N_x} \sum_{k=1}^{N_z} \left(p_{ik}^{c} - m_i \right)^2 \quad \text{.....} \tag{5.2}$$

Where, p_{ik}^{f} is the original given property, p_{ik}^{c} is the intermediate property value after coarsening some layers, m_i is the weighted average of the properties in z-direction.

Before moving to the optimal number of segments, we need to think about how we select two segments to combine. In recursive coarsening technique, first we combine original segments into coarser segments using two adjacent segments at a time. We then calculate sum of squares of variances for each combination of two neighbor segments and pick up the best combination that gives minimum changes within a segments and maximum variance between segments to maintain their heterogeneity. Although the original 'upgridding' idea utilizes permeability as the parameters to evaluate variance, what kind of properties is useful for our streamline application? We use slowness which is the reciprocal of the local velocity, $s = 1/\sqrt{v_x^2 + v_y^2 + v_z^2}$, because this property determines the time of flight along streamlines. As slowness increases, the time of flight increases. Conversely, as slowness decreases, the time of flight decreases. Thus, we require keeping finer segments near low slowness region (fast velocity) and can take more coarse segments in large slowness region (low velocity).

Let's think of a simple 1D example as shown in **Fig. 5.4**. Now we have initially four segments with slowness in the range of 0.1~3 which is on top in **Fig.5.4**.

SSW	SSB	Time of Flight: 5	5	5	5
0	17.01	0.1	5	3	0.15
12	5.01	2.55	2.55	3	0.15
2	15.01	0.1	4	4	0.15
2.05	12.96	0.1	5	1.575	1.575

Figure 5.4— 1-D four segments example.

Since there is no coarsening of the segments yet, sum of squares within segments (*SSW*) is going to be zero, whereas sum of squares between segments (*SSB*) is going to be the maximum value. We coarsen left two segments and take arithmetic average for the segments as shown in second row in **Fig.5.4.** Now *SSW* and *SSB* are calculated as follows,

$$p_{ik}^{f} = \{0.1,5,3,0.15 | i = 1, k = 1 \sim 4\},$$

$$p_{ik}^{c} = \{2.55,2.55,3,0.15 | i = 1, k = 1 \sim 4\},$$

$$m_i = (0.1 + 5 + 3 + 0.15)/4 = 2.0625$$

$$SSW = \sum_{i=1}^{1}\sum_{k=1}^{4}\left(p_{ik}^{f} - p_{ik}^{c}\right)^2 = (0.1 - 2.55)^2 + (5 - 2.55)^2 + (3 - 3)^2 + (0.15 - 0.15)^2$$

$$SSB = \sum_{i=1}^{1}\sum_{k=1}^{4}\left(p_{ik}^{c} - m_i\right)^2 = (2.55 - 2.0625)^2 + (2.55 - 2.0625)^2 + (3 - 2.0625)^2 + (0.15 - 2.0625)^2$$

SSW is increased a little, and *SSB* is decreased a little. We do the same kind of coarsening in the middle two segments and right two segments which are shown in **Fig. 5.4**. If we look at *SSW* and *SSB* values carefully, the combination of middle two segments shows the smallest *SSW* and the largest *SSB* values. This means that this case results in the minimum change within the segments and keeps the heterogeneity between segments after coarsening. Thus, we pick up middle two segments to combine and keep this *SSW* and *SSB* as the values of 3 segments. Now we start coarsening left two, and right two segments and compare *SSW* and *SSB* with the 3 segments model. We continue the same procedure until we have just one segment. **Fig. 5.5** shows the relationship of *SSW* and *SSB* when we coarsen 70 segments into 1 segment.

By coarsening some segments, sum of squares within segment (*SSW*) will be increased because the difference within segments will increase by merging neighboring segments and averaging the segment's value. On the other hand, sum of squares between segments (*SSB*) will be decreased because the heterogeneity is reduced shown in **Fig. 5.5**. We will keep original segment's values with the minimum *SSW*, and keep heterogeneity with the maximum *SSB*.

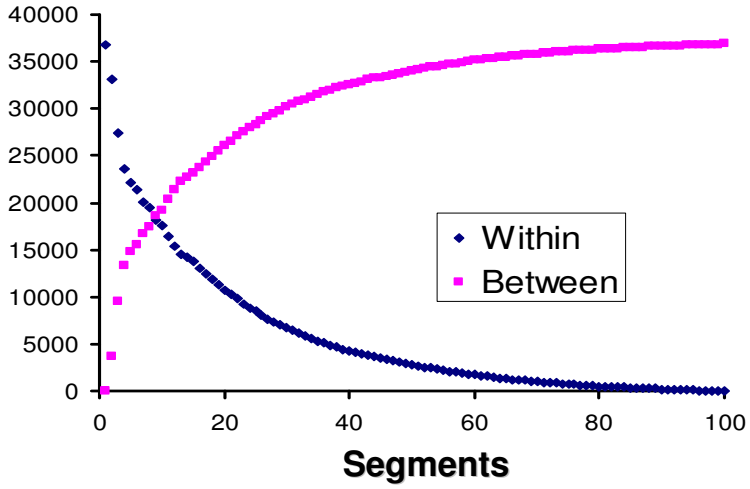

Figure 5.5— Relationship between SSW and SSB.

5.2.2 Determination of Optimal Point

Next step would be how we come up with the optimal number of the coarsening, in other words, when we should stop coarsening. There are three ways to obtain the optimal point. First one would be simply taking the cross point of *SSW* and *SSB* in **Fig. 5.5**. Second way is also quite simple. We will just draw a straight line from *SSB* = maximum value at the minimum number of segment to *SSB* = 0 at the maximum number of segment. The cross point of the straight line and the *SSB* curve would be the optimal one shown in **Fig. 5.6**.

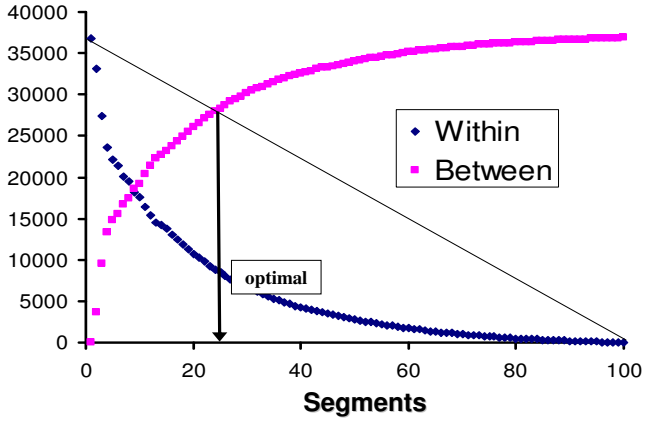

Figure 5.6— Searching optimal point with straight line.

In the third approach, we apply a regression line with the *SSW* vs. the number of segments plot. Starting by drawing the regression line from 3 *SSW* points picked up from the smallest number of segment (1, 2, and 3), we calculate the Root Mean Square Error (RMSE). We can also draw another regression line for the rest of the *SSW* points given by the number of segments from 4~100, then calculate RMSE with the regression line. We add these two RMSE values after normalizing by the number of regression points (100 points in this case) and set as the RMSE result of the number of segment as 3. After that, we increase the number of regression points one by one from the smallest number of segments and obtain **Fig. 5.7**. The smallest RMSE would be the optimal point to finish the coarsening.

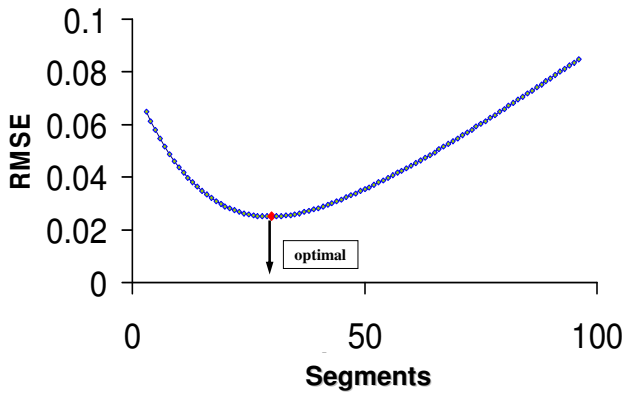

Figure 5.7— Searching optimal point with multiple regression lines.

5.3 Illustration of the Method

We now illustrate the method using a 1-D homogeneous CO2 injection problem with the same fluid properties as in the last chapter. **Figs. 5.8 ~ 5.10** are obtained from this example, and we can see the optimal segments are found to be 35, 35, and 39 respectively.

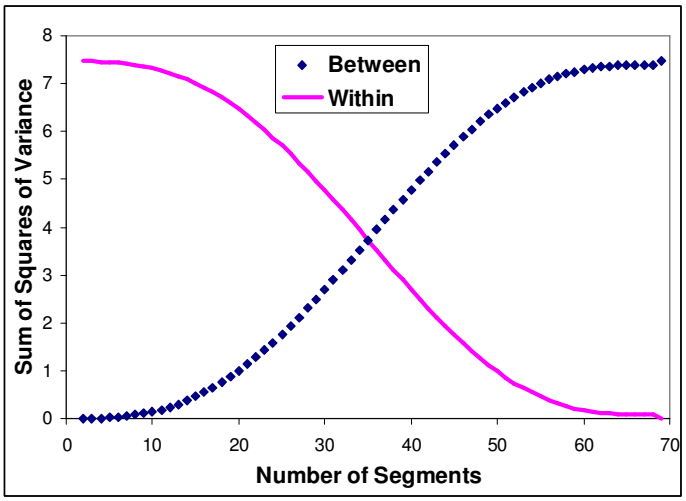

Figure 5.8— Relationship between SSW and SSB.

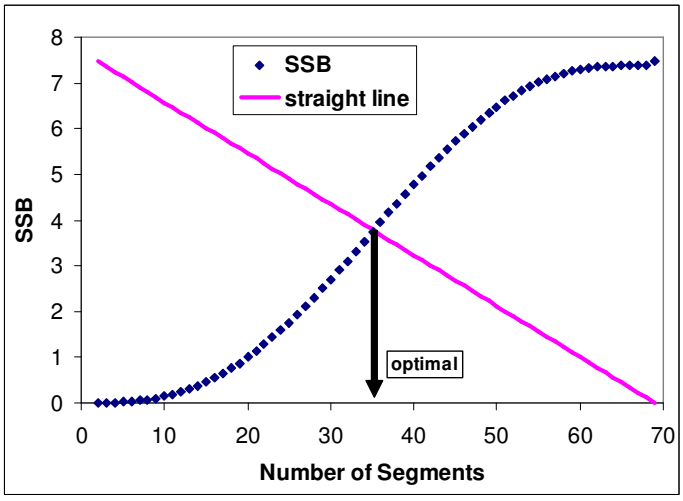

Figure 5.9— Optimal point selection with straight line.

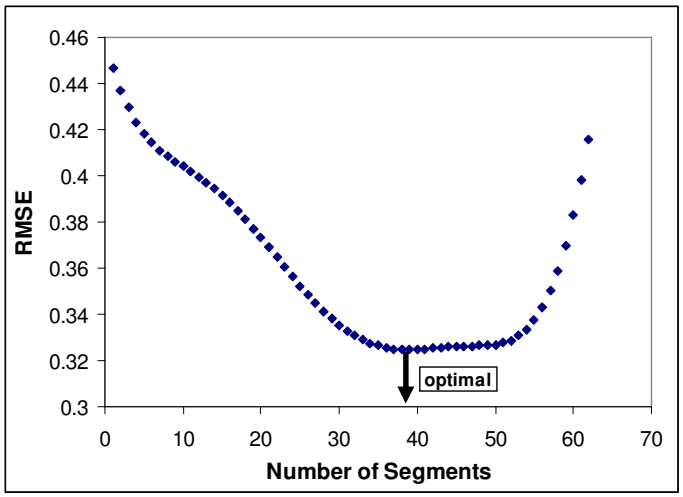

Figure 5.10— Optimal point selection with regression line.

Figs. 5.11 show the comparison of the original grid block slowness and those of the refined segments along the streamline. **Fig. 5.11a** shows results without the optimal coarsening where we have used a factor of 4 to refine the discretization of segments along streamlines. **Fig. 5.11b** shows results with the optimal coarsening method. It is clear that with optimal coarsening we still capture the original grid slowness with a much coarsened segments, especially in high slowness regions with low total velocities. We show 4 different results of gas saturation values as a function of distance from the injection well in **Fig. 5.12**. These 4 different results are from finite difference, streamline simulations without optimal coarsening (refinement factor of 2 and 4), and using optimal coarsening method with an initial refinement factor of 4. As we can see, the results with the refinement factor of 2 deviates from the other three results. It means that the refinement factor is too low to obtain accurate results. The optimal coarsening method was using about the same number of segments as with the refinement factor of 2 after coarsening and still keeps the result very close to the reference solution. Remember that the main objective for the optimal coarsening is to reduce the computational time by reducing the number of flash calculations which require high computational expense during compositional simulation. **TABLE.5.1** summarizes the CPU time for these results. Even for this simple 1-D calculation, we can clearly see the effectiveness of the optimal coarsening method.

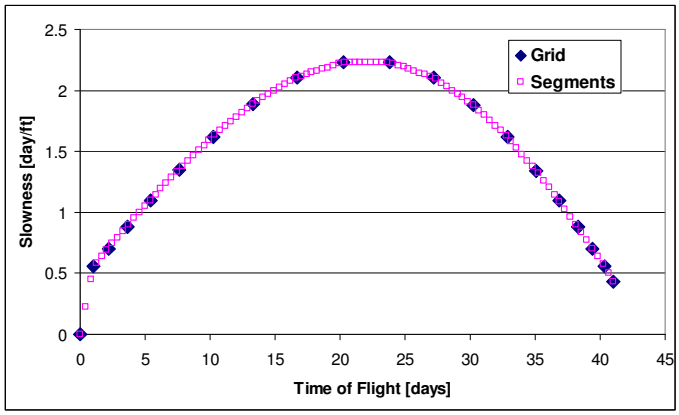

(a) With refinement factor of 4

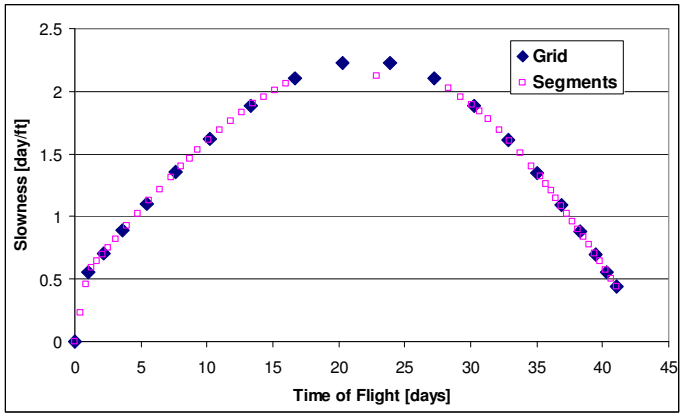

(a) With optimal coarsening

Figure 5.11— Original grid and streamline segments property comparison.

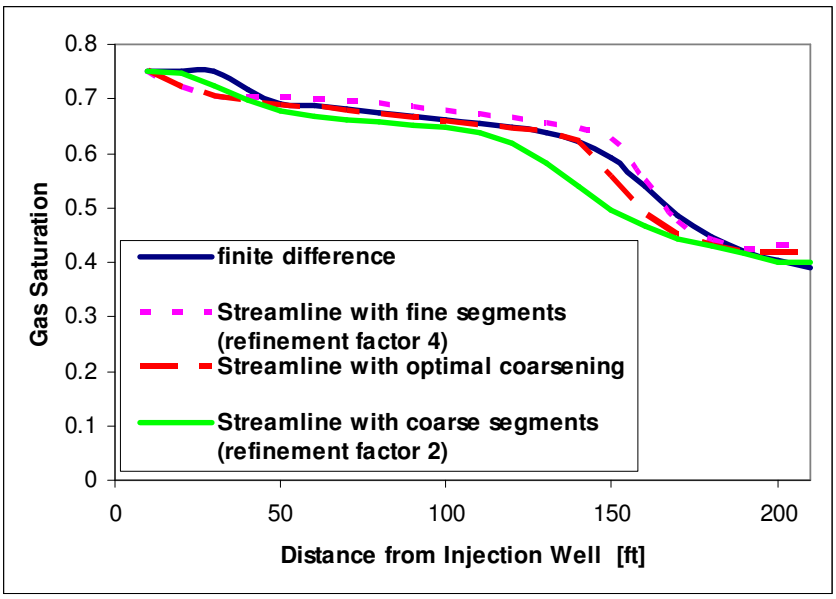

Figure 5.12— 1-D gas saturation profile.

TABLE 5.1 CPU TIME COMPARISONS FOR 1-D OPTIMAL COARSENING

	CPU time [sec]
UTCOMP	46.2465
With Optimal Coarsening	38.5955
Without Optimal Coarsening	60.27667

5.4 Applications

We utilize the same case used in the validation of the method for compressible compositional formulation to show how the optimal coarsening method works. **Fig. 5.13** shows the spatial distribution of gas saturation with the optimal coarsening method. On comparing **Figs. 5.1, 5.3,** and **5.13**, we see that the optimal coarsening method keeps the same higher resolution as the finer discretization of segments and shows a better match with the finite difference solution than a uniformly coarse discretization. For this comparison, the CPU time is also summarized in **TABLE 5.2**. The streamline simulation with the optimal coarsening method doesn't show much faster CPU time than the finite difference simulation for this small example. However compared to the fine-scale solution, it is much faster. The CPU time comparison with finite difference and its scaling properties will be discussed later.

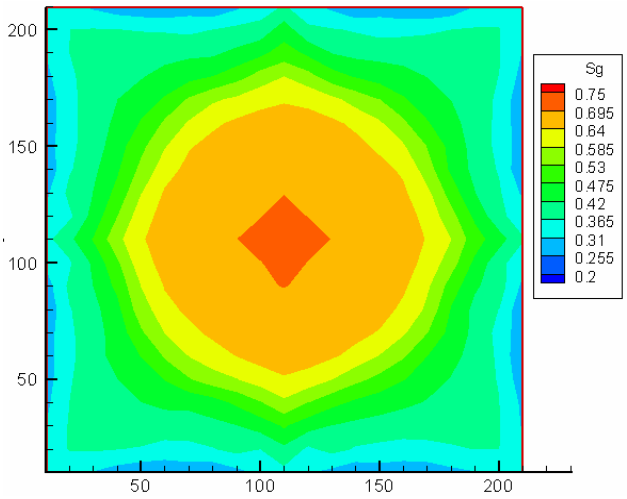

Figure 5.13— Spatial distribution of gas saturation.

TABLE 5.2 CPU TIME COMPARISONS FOR 2-D EXAMPLE

	CPU time [min]
Finite Difference	5
With Optimal Coarsening	15
With Fine Descretization	32
With Coarse Descretization	8

5.5 Scaling of CPU Time

In this section, we investigate the scaling of the CPU time with number of grid blocks for streamline simulation compared to the finite difference compositional simulation. We use 21x21, 51x51, 101x101, and 101x101x3 grid blocks to run a total of 2000 days of simulation. Results are shown in **Fig 5.14**. Because of maximum allowable dimension restrictions for the finite difference simulator, we draw regression lines based on our four cases and extend these lines to larger number of grid blocks. We can see the computational advantage of streamline methods for more than 10000 grid blocks, and especially for about million cells for which streamline method has about 10 times computational speed advantage compared to finite difference simulator.

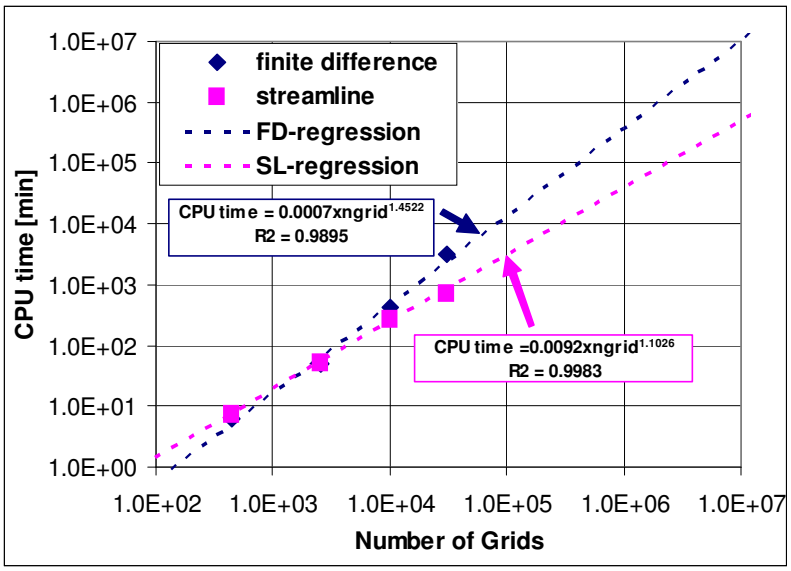

Figure 5.14— CPU time comparison.

5.6 Chapter Summary

We propose a scheme for coarsening of segments for 1-D solution during compositional streamline simulation. As the reservoir size and the number of wells are increased, the number of streamlines used in the model will also be increased. If we want to optimize the number of segments by using the dynamic way like the adaptive mesh algorithm, the calculation time just for the optimization itself will be very costly. However, our simple statistical method for the optimization is computationally efficient. The static optimization is not only giving high quality results comparable to fine segments, it also gives a quantitative analysis by introducing *SSW* and *SSB* to indicate how much heterogeneity and original properties are preserved. We show the effectiveness of the approach and the effectiveness through several synthetic examples. CPU time comparison promises our compositional streamline formulation with optimal coarsening method can be very effective for field-scale high resolution compositional simulation with multimillion cells.

CHAPTER VI

CONCLUSIONS AND RECOMMENDATIONS

6.1 Conclusions

We have presented a rigorous formulation for two and three – phase black oil and compositional streamline simulation. Unlike previous studies, we no longer assume that volumetric flux is conserved along streamlines. The key features of our formulation are (i) introduction and tracing of an effective density along streamlines to account for fluid expansion/compression, (ii) use of the effective density during mapping from streamlines to grid blocks and vice versa and (iii) a source/sink term in the saturation equation along streamlines to account for compressibility effects. Gravity effects are accounted for using operator splitting as in incompressible streamline simulation.[4] We have validated our approach by comparison with finite difference simulation for two and three phase flow using synthetic and field examples. Importantly, our proposed formulation can be easily implemented within the framework of existing streamline simulators.

Some specific conclusions from this study can be summarized as follows:

1. A rigorous compressible streamline formulation has been presented for two and three-phase black oil and compositional simulation. Our proposed approach requires only minor modifications to current streamline simulators with significant improvement in accuracy of performance predictions.
2. We can now account for fluid expansion/compression along streamlines by introducing an effective density along the streamlines. This effective density can be easily traced along the streamline and allows us to rigorously decouple the 3-D saturation/composition equation into a series of 1-D equations.
3. We have reformulated the 1-D saturation/composition equations along streamlines by introducing a source/sink term to account for compressibility effects. Also, the mapping of saturations/compositions from streamlines to grid blocks and vice versa has been improved to account for changes in fluid volume.

4. We have shown that the discrete CFL number of Osako *et al.*[14] for selection of time step for pressure updates also applies to compressible streamline simulation for the black oil model. As expected, the compressible formulation restricts the simulation to smaller time-step size compared to incompressible flow in order to maintain the stability of the solution.
5. We have validated our new formulation using synthetic and field examples and comparison with a commercial finite difference simulator.
6. We have defined an optimal coarsening method for selection of the number of segments along streamline for 1-D solution. The method is easy to apply and can result in significant reduction of computational time while retaining the accuracy of fine discretization.

6.2 Recommendations

Our study is concentrated to overcome the inherent incompressible assumption of current streamline models. However, there is another inherent problem in current streamline models that is mapping error from physical space to streamline co-ordinates. Managing mapping errors using appropriate numerical methods can be an area of future research.

By combining accuracy and computational advantages of streamline simulation in compositional simulation, high resolution simulation of EOR processes and compositional history matching will also be attractive research topic.

NOMENCLATURE

$\vec{a}$	streamline face area vector
$\boldsymbol{B}$	formation volume factor, phase P=Oil, Water, Gas
$\boldsymbol{C}$	divergence of total flux
c_f	formation compressibility
$\boldsymbol{F_P}$	fractional flow, phase *P*=Oil, Water, Gas
$\boldsymbol{g}$	gravity constant
$\boldsymbol{k}$	permeability
$\boldsymbol{k_{rP}}$	relative permeability, phase *P*=Oil, Water, Gas
$\vec{\vec{K}}$	dispersion tensor
$\boldsymbol{M}$	mobility ratio
$\boldsymbol{N_i}$	total number of moles, *i* = number of component
$\vec{n}_f$	cell face area vector (normal)
$\hat{n}$	cell face area vector (unit normal)
$\boldsymbol{P}$	pressure
$\boldsymbol{P_c}$	capillary pressure
$\boldsymbol{PV}$	cell pore volume
$\boldsymbol{q}$	volumetric flux
$\boldsymbol{R_s}$	solution gas oil ratio
$\boldsymbol{S_P}$	water saturation, phase *P*=Oil, Water, Gas
$\boldsymbol{S_{orw}}$	residual oil saturation
$\boldsymbol{S_{wirr}}$	irreducible water saturation
$\boldsymbol{t}$	time
$\boldsymbol{t_1}$, $\boldsymbol{t_2}$	time split times
$\boldsymbol{V_t}$	total fluid volume
$\boldsymbol{V_P}$	rock pore volume
$\boldsymbol{V_b}$	rock bulk volume
$\boldsymbol{W_i}$	number of moles per unit bulk volume, *i* = number of component
$\boldsymbol{x_{ij}}$	mole fraction, *i* = number of component, *j* = phase

$\vec{u}$	total Darcy velocity
$\vec{u}_0$	initial total Darcy velocity
Δt	time step size
Δx	cell size (one-dimensional)
λ_P	mobility, phase *P*=Oil, Water, Gas
τ	time of flight
ϕ	porosity
ρ	relative density
ρ_P	phase density, phase *P*=Oil, Water, Gas
ψ, χ	bi-streamfunctions
μ_p	viscosity, phase P=Oil, Water, Gas
λ_t	total mobility
ξ_j	density, j = phase

REFERENCES

1. Datta-Gupta A. and King M.J.: "A Semianalytic Approach to Tracer Flow Modeling in Heterogeneous Permeable Media," *Adv. in Water Resources*, **18** (1), 9 (1995).
2. Chen, H., Osako, I., Datta-Gupta, A., and King, M.J., "A Rigorous Compressible Streamline Formulation for Two- and Three- Phase Black-Oil Simulation," SPE 96866 Presented at the SPE Annual Technology Conference and Exhibition held in Dallas, TX, 9-12 September 2005.
3. Coats, K.H., "An Equation of State Compositional Model," *Soc. Pet. Eng. J.*, **20**(5), 363-376, 1980.
4. Nghiem, L.X., Fong, D.K., Aziz, K., "Compositional Modeling with an Equation of State," *Soc. Pet. Eng. J.*, **21** (6), 687-698, 1981.
5. Young, L.C., Stephenson, R.E., "A Generalized Compositional Approach for Reservoir Simulation," *Soc. Pet. Eng. J.*, **23** (5), 727-742, 1983.
6. UTCOMP-3.8, "An Equation of State Compositional Simulator," Center for Petroleum and Geosystems Engineering, The University of Texas at Austin (1993).
7. Testerman, J. D., "A Statistical Reservoir-Zonation Technique," *Journal of Petroleum Technology*, 889-893, August 1962.
8. King, M. J. and Datta-Gupta A., Streamline simulation: A current perspective, *In Situ*, **22**(1), 91-140, 1998.
9. Datta-Gupta, A., "Streamline Simulation: A Technology Update," SPE Distinguished Author Series, *Journal of Petroleum Technology*, 68-73, December 2000.
10. Bratvedt, F., Gimse, T. and Tegnander, C., "Streamline Computations for Porous Media Flow Including Gravity," *Transport in Porous Media*, 25, 63, 1996.
11. Thiele, M. R., Batycky, R. P. and Blunt, M. J., "A Streamline-Based 3D Field-Scale Compositional Reservoir Simulator" SPE 38889 Presented at the SPE Annual Technical Conference and Exhibition held in San Antonio, TX, 5-8 October, 1997.
12. Ponting, D. K., "Hybrid Streamline Methods," SPE 39756, presented at the 1998 Asia Pacific Conference on Integrated Modeling, Kuala Lumpur, Malaysia, 23-24 March, 1998.

13. Ingebrigtsen, L., Bratvedt, F. and Berge, J., " A Streamline Based Approach To Solution of Three-Phase Flow," SPE 51904 Presented at the 1999 SPE Reservoir Simulation Symposium held in Houston, TX, 14-17 February 1999.
14. Jessen, K. and Orr, F. M., "Compositional Streamline Simulation," SPE 77379 Presented at the SPE Annual Technical Conference and Exhibition, San Antonio, TX, Sept. 29-Oct. 2, 2002.
15. Crane, M., Bratvedt, F., Bradvedt, K., Childs, P. and Olufsen, R., "A Fully Compositional Streamline Simulator," SPE63156 Presented at the SPE Annual Technical Conference and Exhibition held in Dallas, TX, 1-4 October 2000.
16. Bear, J., Dynamics of Fluid in Porous Media, *Dover Publications*, New York (1973).
17. Pollock, D. W., "Semianalytical Computation of Path Lines for Finite-Difference Models," *Ground Water*, **26**(6), November-December, 1988.
18. Lake, L. W., Enhanced Oil Recovery, *Prentice Hall*, Englewood Cliffs, NJ (1989).
19. Sammon, P. H. "An Analysis of Upstream Differencing," *SPERE*, 1053-1056, August 1988.
20. He, Z., Yoon, S., and Datta-Gupta, A. "Streamline-based Production Data Integration With Gravity and Changing Field Conditions," *SPE Journal* , **7** (4), p423-436, December 2002.
21. Osako, I., Datta-Gupta, A. and King, M. J.," Timestep Selection During Streamline Simulation Through Transverse Flux Correction," *SPE Journal*, **9** (4), p450-462, December 2004.
22. Coats, K. H., "IMPES Stability: The CFL Limit," SPE 66345 presented at the SPE Reservoir Simulation Symposium, Houston, TX, 11-14 February, 2001.
23. Martin, J. C. and Wegner, R. E., "Numerical Solution of Multiphase Two-Dimensional Incompressible Flow Using Streamtube Relationships," *Soc. Pet. Eng. J.*, **19**, 313 (1979).
24. Bratvedt, F., Bratvedt, K., Buchholz, C. F., Gimse, T., Holden, H., Holden, L. and Risebro, N. H., "FRONTLINE and FRONTSIM. Two Full Scale, Two-Phase, Black Oil Reservoir Simulators Based on Front Tracking," *Surv. Math. Ind.*, **3**, 185 (1993).
25. Bratvedt, F., Bratvedt, K., Buchholz, C. F., Holden, L., Holden, H. and Risebro, N. H., A New Front Tracking Method for Reservoir Simulation, *SPE Reser. Eng.*, 7, 107 (1992).
26. Crane, M. J. and M. J. Blunt, Streamline-based simulation of solute transport, *Water Resour. Res.*, **35**(10), 3061-3078, 1999.

27. Behrens, R. A., Jones, R. C. and Emanuel, A. S., "Implementation of a Streamline Method for Flow Simulation of Large Fields," *Journal of Canadian Petroleum Technology*, Special Edition, **38** (13), 1999.
28. Jessen, K. and Orr, F. M., "Gravity Segregation and Compositional Streamline Simulation," SPE89448 Presented at the 2004 SPE/DOE Fourteenth Symposium on Improved Oil Recovery held in Tulsa, Oklahoma, 17-21 April 2004.
29. Berenblyum,R. A., Shapiro, A. A., Jessen, K., Stenby, E. H., Orr, F. M., " Black Oil Streamline Simulator with Capillary Effects," Presented at SPE Annual Technology Conference and Exhibition held in Denver, Colorado, 5-8 October, 2003.
30. Acs, G., Doleschall, S., and Farkas, E., "General Purpose Compositional Model," *SPE Journal,* p543-558, August 1985.
31. Watts, J. W., "A Compositional Formulation of the Pressure and Saturation Equations," *SPERE*, p243-252, May 1986.
32. Chang, Y., "Development and Application of An Equation of State Compositional Simulator," Ph.D Dissertation, The University of Texas, 1990.
33. Baker, L. E., Pierce, A. C., and Luks, K. D., "Gibbs energy analysis of phase equilibria," *SPE Journal*, **22**, p731-742, 1982.
34. Michelsen, M. L., "The isothermal flash problem Part I: stability," *Fluid Phase Equilib*, **9**, p1-19, 1982.
35. Trangenstein, J. A., "Numerical Analysis of Reservoir Fluid Flow, Multiphase Flow in Porous Media: Mechanics, Mathematics and Numerics, " Lecture Notes in Engineering, *Springer Verlag* (**34**), p87-246, 1987
36. Peng, D.Y., and Robinson, D. B., "A New Two-Constant Equation of State," *Industrial and Engineering Chemistry: Fundamentals*, **15**, p59-64, 1976
37. Jessen, K., Wang, Y., Ermakov, P., Zhu, J., and Orr, F. M., "Fast, Approximate Solutions for 1D Multicomponent Gas-Injection Problems," *SPE Journal*, **6** (4), p442-451, December 2001.
38. Mallison, B. T., Gerritsen, M. G., Jessen, K., and Orr, F. M., "High- Order Upwind Schemes for Two-Phase, Multicomponent Flow," *SPE Journal*, **10** (3), p297-311, December 2005.
39. Johns, R. T., and Orr, F. M., "Miscible Gas Displacement of Multiplecomponent Oils," *SPE Journal*, p39-50, March 1996.

40. Dindoruk, B., Orr, F. M., and Johns, R. T., “Theory of Multicomtact Miscible Displacement with Nitrogen,” *SPE Journal*, **2**, p268-279, September 1997.
41. Gardner, J. W., and Ypma, J.G.J., “An Investigation of Phase Behavior-Macroscopic Bypassing Interaction in CO2 Flooding,” *SPE Journal*, 508-541, October 1984
42. Datta-Gupta, A., Lake, L. W., Pope, G. A., Sepehrnoori, K. and King, M. J., "High Resolution Monotonic Schemes for Reservoir Fluid Flow Simulation," *In Situ*, **15** (3), 289-317, 1991.
43. Harten, A., “High Resolution Schemes for Hyperbolic Conservation Laws,” *J. Comput. Phys*., 49, 357–393, 1983.
44. Leonard, B. P., “A Stable and Accurate Convective Modeling Procedure Based on Quadratic Upstream Interpolation,” *Comput. Methods Appl. Mech. Eng*., **19**, 59-98, 1979.
45. Sweby, P. K., "High-resolution Schemes Using Flux Limiters for Hyperbolic Conservation-laws.", *Siam J. Numer. Analysis*, **21**, pp995-1011, 1984.
46. Sammon, P. H., “Dynamic Grid Refinement and Amalgamation for Compositional Simulation,” SPE 79683 Presented at the SPE Reservoir Simulation Symposium held in Houston, TX, February 2003.
47. Li, D., and Beckner, B., “Optimal Uplayering for Scaleup of Multimillion-Cell Geologic Models,” SPE 62927 Presented at the SPE Annual Technology Conference and Exhibition held in Dallas, TX, 1-4 October 2000.
48. Li, D., Cullick, A. S., and Lake, L. W., “Global Scale-Up of Reservoir Model Permeability with Local Grid Refinement,” *Journal of Petroleum Science and Engineering*, **14**, 1-13, 1995.

VITA

Ichiro Osako received his B.Eng. degree in environmental and mineral resources engineering from Waseda University, Tokyo, Japan, in March 2001, M.S and Ph.D degree in Petroleum Engineering from Texas A&M University in December 2003, December 2006 respectively.

His permanent address: 339 Asano
Munakata, Fukuoka
Japan, 811-3415